ISSN 0006-2979, Biochemistry (Moscow), 2024, Vol. 89, No. 8, pp. 1362-1391 © The Author(s) 2024. This article is an open access publication.

REVIEW

Development of Graphene-Based Materials with the Targeted Action for Cancer Theranostics

Konstantin N. Semenov[1,2,3,a]*, Olga S. Shemchuk[1,2], Sergei V. Ageev[1,2], Pavel A. Andoskin[1], Gleb O. Iurev[1], Igor V. Murin[2], Pavel K. Kozhukhov[2], Dmitriy N. Maystrenko[3], Oleg E. Molchanov[3], Dilafruz K. Kholmurodova[4], Jasur A. Rizaev[4], and Vladimir V. Sharoyko[1,2,3,b]*

[1]*Pavlov First Saint Petersburg State Medical University, 197022 Saint Petersburg, Russia*
[2]*Saint Petersburg State University, 199034 Saint Petersburg, Russia*
[3]*Granov Russian Research Centre for Radiology and Surgical Technologies, 197758 Saint Petersburg, Russia*
[4]*Samarkand Medical University, 100400 Samarkand, Uzbekistan*
[a]*e-mail: knsemenov@gmail.com* [b]*e-mail: sharoyko@gmail.com*

Received May 30, 2024
Revised July 11, 2024
Accepted July 13, 2024

Abstract—The review summarises the prospects in the application of graphene and graphene-based nanomaterials (GBNs) in nanomedicine, including drug delivery, photothermal and photodynamic therapy, and theranostics in cancer treatment. The application of GBNs in various areas of science and medicine is due to the unique properties of graphene allowing the development of novel ground-breaking biomedical applications. The review describes current approaches to the production of new targeting graphene-based biomedical agents for the chemotherapy, photothermal therapy, and photodynamic therapy of tumors. Analysis of publications and FDA databases showed that despite numerous clinical studies of graphene-based materials conducted worldwide, there is a lack of information on the clinical trials on the use of graphene-based conjugates for the targeted drug delivery and diagnostics. The review will be helpful for researchers working in development of carbon nanostructures, material science, medicinal chemistry, and nanobiomedicine.

DOI: 10.1134/S0006297924080029

Keywords: graphene, graphene-based nanomaterials, drug delivery, theranostics

INTRODUCTION

Graphene-based nanomaterials (GBNs), such as graphene, graphene oxide (GO), reduced graphene oxide (rGO), and graphene quantum dots (GQDs) (Fig. 1), attract a significant attention due to their structure and physicochemical properties. Some of the promising applications of GBNs in the field of biomedicine include tissue engineering [1], bioimaging [2, 3] targeted drug delivery [4-9], development of biosensors [10-12] and antiviral [13-16], antibacterial [17-20], and antifungal agents [21, 22], and delivery of biomolecules, such as enzymes [23], proteins [24-26], genes [27-29], RNA [30, 31], and DNA [32, 33] (Fig. 2).

GBNs can be modified by covalent [34, 35] and noncovalent [36, 37] functionalization to enhance their electrical [38, 39], optical [40, 41], thermal [42, 43], electronic [44-46], and mechanical [47, 48] properties. Monolayer graphene was first obtained in 2004 by Andre Geim and Konstantin Novoselov [49]. Depending on the method of synthesis, graphene can be produced as mono- or multilayered flakes [50, 51]. It can be synthesized by chemical vapour deposition [52-58], electrochemical exfoliation [59-62], mechanochemical exfoliation [63], and chemical and thermal

Abbreviations: GBNs, graphene-based nanomaterials; CYT, cytostatic drug cytarabine; FA, folic acid; GQDs, graphene quantum dots; HAS, human serum albumin; Pc, phthalocyanine; PEG, polyethylene glycol; PDT, photodynamic therapy; PTT, photothermal therapy; rGO, reduced graphene oxide; ROS, reactive oxygen species.

* To whom correspondence should be addressed.

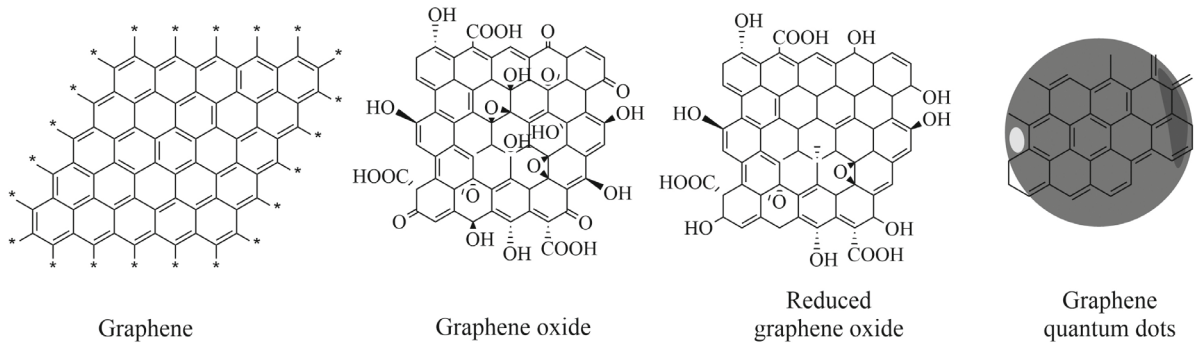

Fig. 1. Classification of GBNs.

reduction of GO (synthesis of rGO) [64-70]. rGO is a GO derivative in which almost all oxygen-containing groups are reduced with hydrazine hydrate or biomolecules [71] (see Fig. S1 in the Online Resource 1 for rGO synthesis from GO using l-cysteine [71]).

Graphene consists of sp^2-hybridised hexagonal carbon atoms that form two-dimensional nanolayers, while GO additionally has oxygen-containing groups on the surface, e.g., carbonyl, lactol, and carboxyl groups at the edges of GO layers and epoxy and hydroxyl groups on the basal plane (Fig. S2 in the Online Resource 1) [72-74].

GBNs can be functionalized with molecules of various nature due to the presence of functional groups on the GO surface and sp^2-hybridised carbon atoms. Reactions that can be carried out on the GO surface (Fig. 3) include amidation, esterification, 1,3-dipolar cycloaddition, and halogenation. Other types of interactions are hydrogen bonding, π–π stacking, and hydrophobic interactions.

GQDs are graphene nanoparticles less than 100 nm in size. Due to their exceptional properties, such as low toxicity, stable photoluminescence, chemical stability, and pronounced quantum confinement effect, GQDs are considered as new promising materials for biology, optoelectronics, energy industry, and environment [75-78]. GQDs can be prepared using top-down or bottom-up approaches (Fig. 4) [79-81].

GBN CONJUGATES IN BIOMEDICINE

GBNs can be effectively used in the antitumor therapy, e.g., for the development of platforms for the delivery of drugs and genetic constructs, photodynamic therapy (PDT), photothermal therapy (PTT), and theranostics (Fig. 5).

To efficacy of GBN-based antitumor nanodrugs can be increased by using specific vectors for their delivery that are developed to recognise tumor-specific receptors, such as HER2, CAIX, and receptors for Tat, LHRH, folate, biotin, and asialoglycoprotein (Fig. 6).

BIOCOMPATIBILITY AND MECHANISMS OF ENDOCYTOSIS

Analysis of publications shows that functionalization of graphene surface decreases hemolysis and, therefore, increases material hemocompatibility.

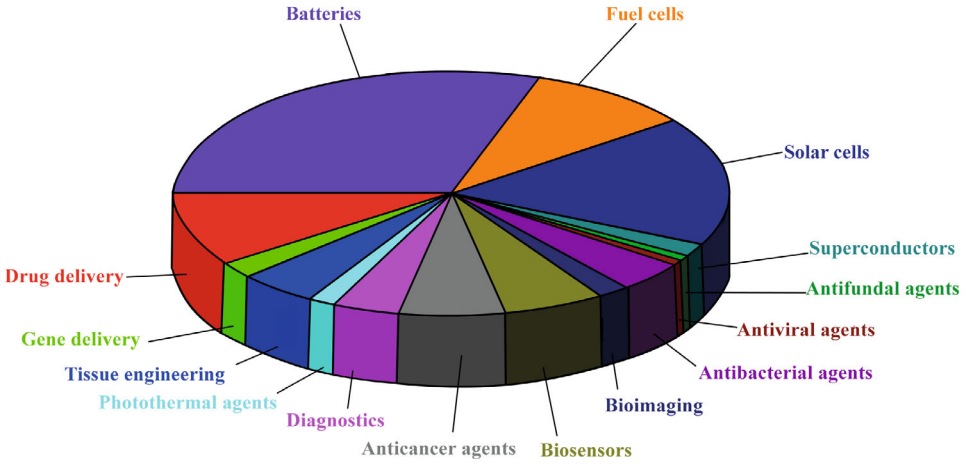

Fig. 2. Publications on GBN applications.

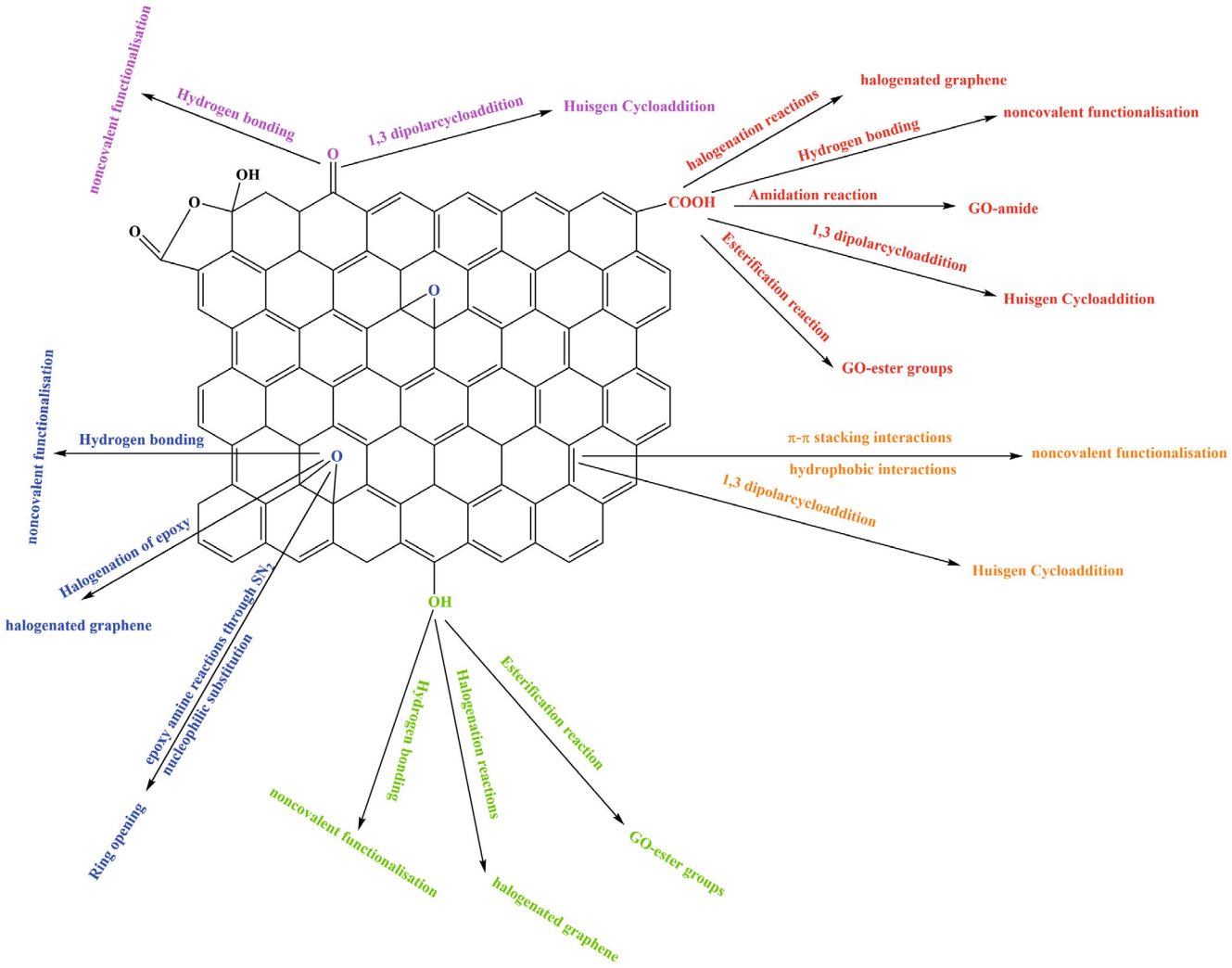

Fig. 3. Reactions carried out on graphene surface.

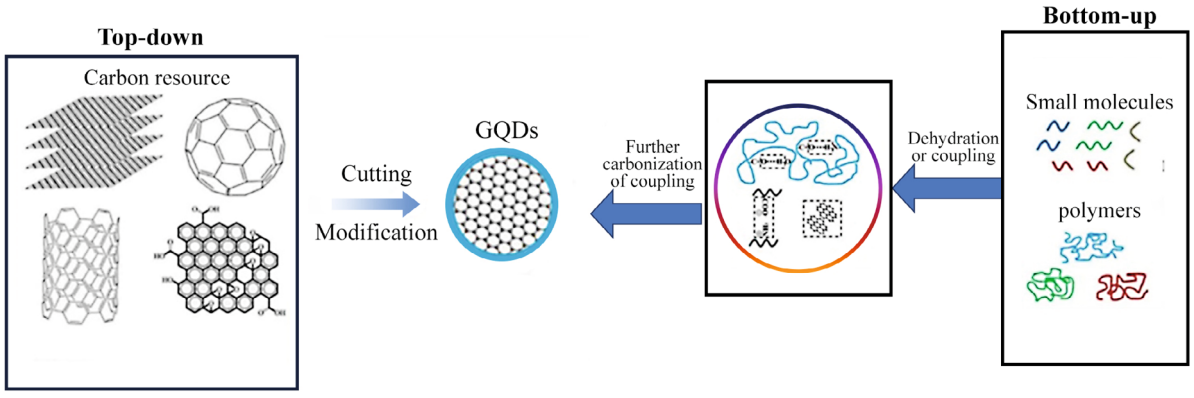

Fig. 4. Approaches for GQD synthesis: top-down degradation from various carbon sources and bottom-up synthesis from small molecules or polymers.

Thus, noncovalent functionalization of GO with chitosan produced a material with no hemolytic activity. Pinto et al. [82] showed that the noncovalent functionalization of graphene surface with polymers [polyvinyl alcohol, polyethylene glycol (PEG), polyvinylpyrrolidone (PVP), hydroxyethylcellulose, chondroitin, glucosamine, and hyaluronic acid (HA)] decreased hemolysis to 1.7% for all the resulting materials at concentrations below 500 μg·ml^{-1}. Previously, we have studied the effect of GO enriched (about 85%) with oxygen-

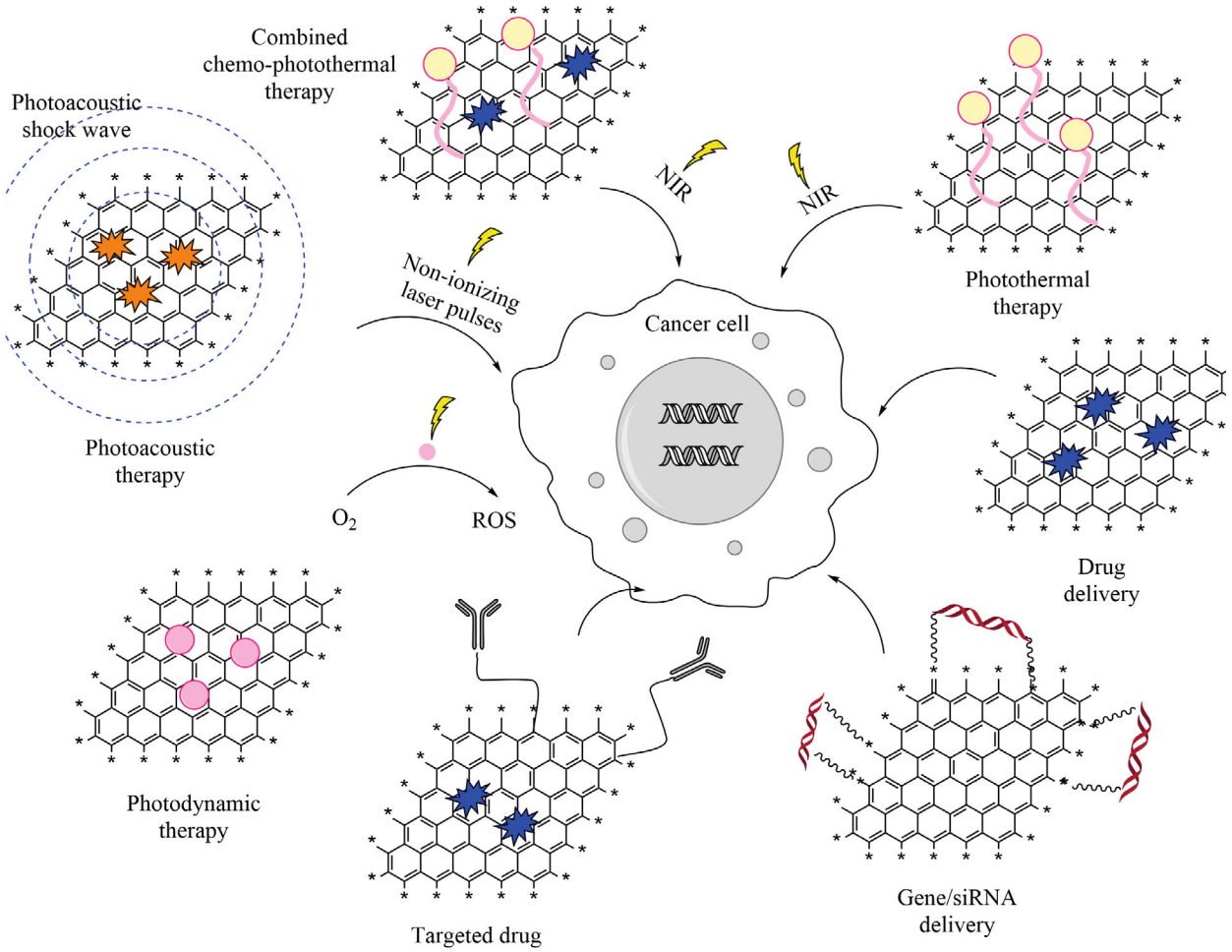

Fig. 5. Application of GBNs in cancer treatment.

containing functional groups (edge-oxidized graphene oxide, EOGO) on the extent of spontaneous hemolysis and found that within the studied concentration range (C_{GO} = 2.5-25 mg·liter^{-1}), this nanomaterial did not affect the level of hemolysis after 1 and 3 h of incubation [83], while, as demonstrated in [84, 85], GO with a lower content of oxygen-containing functional groups (C/O ratio, 2 : 1) caused the rupture of erythrocyte membranes with subsequent release of hemoglobin. Our research group also showed that GO functionalized with L-methionine (GFM) [85], L-cysteine (GFC) [86], glycine (GO-Gly) [87], or folic acid (GO-FA) [88] caused no damage to the erythrocyte membrane at the concentrations up to 25 μg·ml^{-1}.

In comparison with GO, GO functionalized with amino groups caused no activation of platelet aggregation up to C = 2 μg·ml^{-1}. The authors showed that GO-induced aggregation was stronger than the thrombin-induced aggregation [89]. Podolska et al. [90] found that GO, rGO, and rGO-PEG (C = 50 μg mL^{-1}) did not stimulate platelet aggregation in the presence of 2 μmol·ml^{-1} adenosine diphosphate (ADP). GFC (up to 25 μg·liter^{-1}) caused no ADP-induced stimulation of platelet aggregation, while GFM and EOGO demonstrated the antiplatelet activity at the concentrations up to 25 and 100 μg·liter^{-1}, respectively, in experiments on ADP- and collagen-induced aggregation.

Ding et al. [91] showed that GO (dispersion concentration, C = 100 μg·ml^{-1}) interacted with human serum albumin (HSA) through various types of interactions (covalent and hydrogen bonding, electrostatic forces, hydrophobic interactions, and π–π stacking) that resulted in the HSA dysfunction and its inability to remove toxins due to conformational changes, which indicated a potential toxicity of GO. Functionalization of the GO surface with carboxyl groups (GO-COOH) increased its biocompatibility, as GO-COOH caused no functional changes in HSA. In contrast, Taneva et al. [92] found that interaction of GO (8 mg·ml^{-1}) with HSA did not inactivate HSA in the blood plasma because of the low affinity of GO for HSA. We demonstrated that interaction of modified GO (GFM and GFC) with HSA occurred mainly due to the formation of hydrogen bonds: the dissociation constants for the GFM and GFC complexes with HSA were 185.2 [85] and 1600 [86] μg·ml^{-1}, respectively.

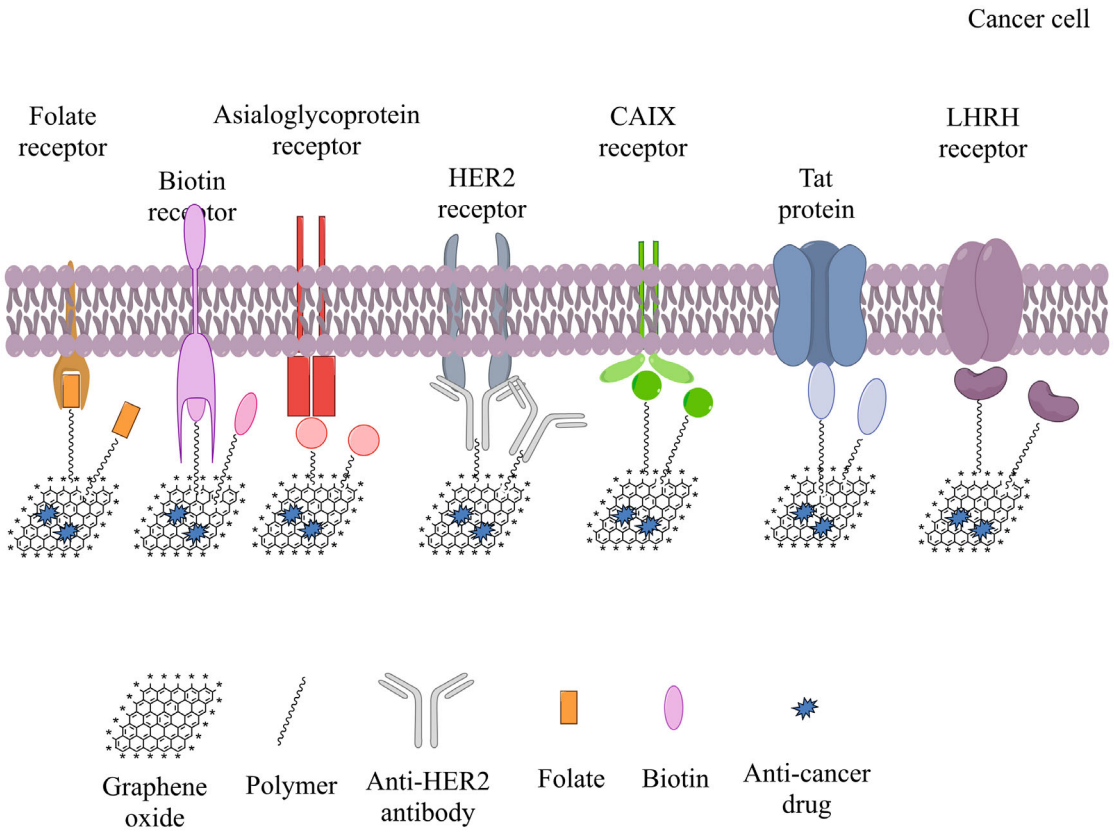

Fig. 6. Tumor-specific receptors and ligands used in GBN modification.

Liu et al. [93] found that GO at the concentrations up to 100 μg ml^{-1} induced mutagenesis due to its effect on DNA replication and gene expression. Wang et al. [94] reported that GO (up to 100 μg·ml^{-1}) displayed a significant genotoxicity toward human lung fibroblasts because of the DNA damage resulting from the generation of reactive oxygen species (ROS) and surface charge of GO. The authors showed that functionalization of the GO surface with PEG and lactobionic acid (LA) significantly reduced the genotoxicity.

Akhavan et al. [95] showed that the genotoxicity depends on the lateral dimensions of graphene: rGO nanoparticles with an average lateral dimension of 11 ± 4 nm were able to penetrate into the nuclei of human mesenchymal stem cells, leading to DNA fragmentation and chromosomal aberrations even at low rGO concentrations (0.1 and 1.0 mg·ml^{-1}) after 1 h of incubation. At the same time, rGO sheets with an average lateral size of 3.8 ± 0.4 μm did not exhibit genotoxicity at a concentration of 100 mg·ml^{-1} after 24-h incubation. Our research group showed that GFM and GFC did not display genotoxicity at the concentrations up to 25 μg·ml^{-1}, while EOGO did not exhibit the genotoxic effect up to C = 100 μg·ml^{-1}. We also studied the mechanism of endocytosis of GO conjugates with 1,3,5-triazine-based cytostatic drugs and showed that the transport of these conjugates could occur via two mechanisms – pinocytosis and clathrin-dependent endocytosis [96].

The possibility of selective delivery of the cytostatic drug cytarabine (CYT) was shown in [88]. Using a conjugate of GO with CYT and folic acid (FA) as a vector molecule, our research group demonstrated that the GO-FA-CYT nanoparticles localized in the vicinity of folate receptor-expressing pancreatic carcinoma cells (PANC-1) (Fig. 7).

DRUG DELIVERY, PHOTOTHERMAL THERAPY (PTT), AND PHOTODYNAMIC THERAPY (PDT)

Below, we will discuss the use of GBNs in tumor chemotherapy. GBNs can be conjugated with anticancer drugs by noncovalent functionalization of the graphene surface (see Table 1).

GBNs exhibit a high photothermal conversion efficiency, i.e., they efficiently convert absorbed light into heat. In particular, they can absorb light in the near-infrared (NIR) region, which is a transparency region for biological tissues (750-1700 nm), thus allowing deep tissue heating [118]. Such localized heating can selectively damage or destroy cancer cells in PTT, representing a minimally invasive medical treatment.

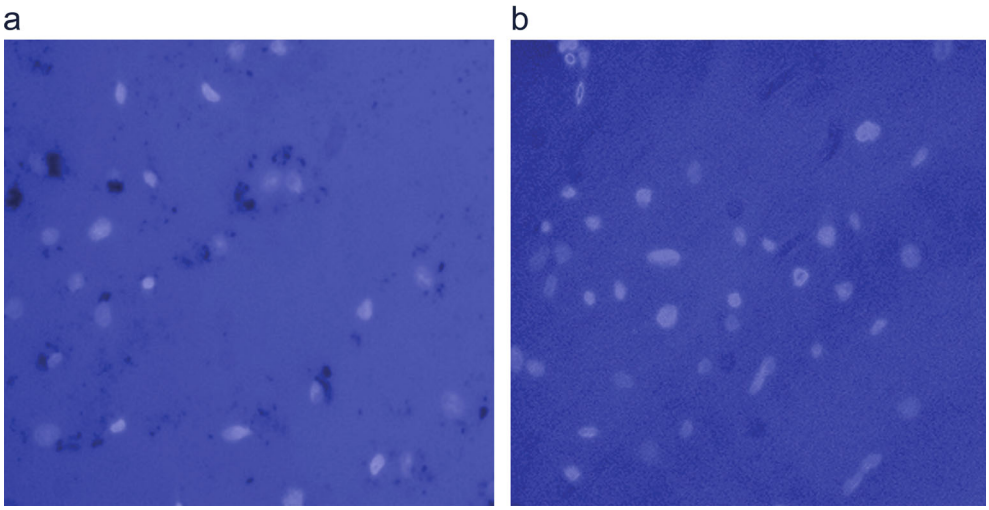

Fig. 7. Fluorescence microscopic images of folate receptor-expressing PANC-1 cells incubated with GO-FA-CYT (a) and GO (b).

The size of GBNs promotes their permeability, retention, and selective clustering at the tumor loci [119]. Table 2 summarises information on the use of GBNs in chemotherapy and PTT.

GO is a highly efficient nanomaterial for PDT, since its irradiation in the NIR region results in the formation of ROS *in situ*, leading to tumor ablation. The presence of functional groups (epoxy, carbonyl, carboxyl, and hydroxyl) on the GO surface allows to load it with drugs, including photosensitisers, which greatly enhances the efficacy of PDT. GQDs have a significant singlet oxygen quantum yield. Because of their properties, such as suitability for bioimaging, drug loading capacity, and high therapeutic efficacy in PDT, they can be used as a multifunctional nanoplatform in theranostics. These properties also create the possibility of using GBNs in the treatment of cancer. Table 3 summarises the data on the use of GBNs in PDT.

DESIGN OF GBN-BASED THERANOSTIC APPROACHES

Hatamie et al. [161] synthesized GO/cobalt nanocomposites for inducing magnetic fluid hyperthermia (MFH) and as contrast agents in magnetic resonance imaging (MRI) [162]. The composites were obtained by chemical synthesis (using GO as a source material) and assembly of 15-nm cobalt nanoparticles; the concentration of cobalt in the nanocomposites was 80%. The studies of hyperthermia induction showed a superior conversion of electromagnetic energy into heat at a frequency of 350 kHz for the nanocomposite dispersions with the concentrations of 0.01 and 0.005 g/liter. MRI showed that negatively charged GO/cobalt nanocomposites were suitable for T1-weighted imaging.

Su et al. [163] engineered a noncovalent based mitomicine C–graphene–BODIPY (4,4-difluoro-4-bora-3a,4a-diaza-s-indacene)–mPEG (MGBP) nanoconjugate that ensured extensive ROS production and high photothermal conversion efficiency (48%) and demonstrated an excellent therapeutic efficacy *in vitro* (decreased HeLa cell viability to 17%). Apart from the synergistic photo/chemo therapy, MGBP can be used in fluorescence and photothermal dual-mode imaging, as BODIPY emits fluorescence when exposed to laser irradiation (see Fig. S3 in the Online Resource 1 for the use of MGBP in theranostics).

Taratula et al. [164] reported a novel cancer-targeting nanoplatform for imaging and treatment of unresected ovarian cancer tumors by intraoperative multimodal phototherapy. To develop this theranostic system, low-oxygen-containing graphene nanosheets were chemically modified with polypropylenimine dendrimers loaded with phthalocyanine (Pc) as a photosensitiser. Such molecular design prevented the quenching of Pc fluorescence by graphene nanosheets, providing the possibility of fluorescence imaging. Furthermore, the developed nanoplatform was conjugated with PEG to improve its biocompatibility and with luteinising hormone-releasing hormone (LHRH) peptide for the tumor-targeted delivery (Fig. S4 in the Online Resource 1). Notably, a low-power NIR irradiation at a single wavelength was used for both heat generation by the graphene nanosheets (PTT) and ROS production by Pc (PDT). Such combinatorial phototherapy resulted in an enhanced destruction of ovarian cancer cells, with a killing efficacy of 90-95% at low doses of Pc and low-oxygen-containing graphene, presumably, due to the synergistic cytotoxic effect of generated ROS and mild hyperthermia. *In vivo* studies confirmed that Pc loaded into this nanoplatform can be employed as a NIR fluorescence agent for the imaging-guided drug delivery.

Table 1. Cytotoxicity of GBN conjugates with cytostatic drugs in *in vitro* experiments

Type of carbon nanoconjugate	Drug load	Cell lines or type of cancer	Applied concentrations and IC_{50} or cytotoxicity (approx. %) at the highest concentration	References
GO with FA-modified β-cyclodextrin (CD) (GO–FA–β-CD)	doxorubicin (DOX), 168%	HeLa	71% inhibition	[97]
Ultrasmall nano-GO (NGO) with covalent grafting of PEG and covalently conjugated B cell-specific antibody Rituxan (RB) (NGO–PEG–RB)	DOX, 40%	Raji	80% inhibition	[98]
GO with adriamycin (ADR) (GO–ADR)	ADR, 93.6%	MCF-7 MCF-7/ADR	IC_{50} = 1.28 ± 0.26 μg/ml (MCF-7) IC_{50} = 13.95 ± 0.53 μg/ml (MCF-7/ADR)	[99]
Hybrid of graphene nanosheets (GNSs), carbon nanotubes (CNTs), and iron oxide nanoparticles (GNS–CNT–Fe_3O_4)	0.27 mg/mg at 5-fluorouracil (5-FU) concentration of 0.5 mg/ml	HepG2	28% viability at 80 μg/ml	[100]
Polyethyleneimine (PEI)-functionalized GO (GO–PEI, covalent)	n/a	HeLa	IC_{50} = 1.3 μg/ml (GO–PEI/scrambled siRNA) IC_{50} = 1.3 μg/ml (GO–PEI/Bcl-2-targeting siRNA)	[101]
NGO–PEG (noncovalent)	1 g of NGO–PEG loaded ~0.1 g of SN-38 (7-ethyl-10-hydroxycamptothecin)	HCT-116	IC_{50} = 6 nM	[102]
NGO covalently modified with diazonium salt of *p*-aminobenzenesulfonic acid (NGO–SO_3H)	DOX, more than 400%	MCF-7	NGO-SO_3H-DOX Relative viability of 75% after 48 h at 20 μg/ml (in terms of DOX)	[103]
NGO covalently modified with diazonium salt of *p*-aminobenzenesulfonic acid and FA (NGO-FA)	DOX, more than 400%; camptothecin (CPT) 4.5 %	MCF-7	NGO-FA-DOX Relative viability of 30% after 48 h at 20 μg/ml (in terms of DOX) NGO-FA-CPT/DOX Relative viability of 80 % after 48 h at 200 ng/ml (in terms of CPT) NGO-FA-CPT Relative viability of 80 % after 48 h at 200 ng/ml (in terms of CPT)	[104]
GO–chlorotoxin (CTX) (GO–CTX, noncovalent)	570 mg DOX per 1 g of GO–CTX	C6	*C* = 1-5 μg/ml % of cytotoxicity, 60%	[104]
GO–sodium alginate (SA) (GO–SA, covalent)	1.8 mg of DOX per 1 mg of GO–SA	HeLa	*C* = 5-20 μg/ml % of cytotoxicity, 69%	[105]
GO nanoplatelets (GONPs), 50 × 50 nm^2	Cisplatin (CP) loading was not determined	A549	*C* = 2.5-30 μg/ml % of cytotoxicity = 90%	[106]

Table 1 (*cont.*)

Type of carbon nanoconjugate	Drug load	Cell lines or type of cancer	Applied concentrations and IC_{50} or cytotoxicity (approx. %) at the highest concentration	References
GO–PEG–FA (noncovalent)	CPT, 45%	MCF-7	*C* = 20-100 μg/ml % of cytotoxicity, 76%	[107]
GO–Fe_3O_4–β-CD (covalent)	DOX, 37.4%; methotrexate (MTX), 23.4%	K562	*C* = 2-16 μg/ml; % of cytotoxicity (DOX), 65% % of cytotoxicity (MTX), 55%	[108]
GO–PEG–FA (noncovalent)	protocatechuic acid (PCA), 23.47%; chlorogenic acid (CA), 18.33%	HT29, HepG2	*C* = 1.56-100 μg/ml % of cytotoxicity (HT29), 58%; IC_{50} (HT29) = 50.69 μg/ml % of cytotoxicity (HepG2), 61% IC_{50} (HepG2) = 40.39 μg/ml	[109]
GO–FA–bovine serum albumin (BSA) (covalent)	DOX, 437.43 μg per 1 mg of GO–FA–BSA	MCF-7 (FA-receptor-positive) A549 (FA-receptor-negative)	*C* = (0.01-20) μg/ml IC_{50} (MCF-7, 24 h) = 8.9 ± 0.7 μg/ml IC_{50} (MCF-7, 48 h) = 0.048 ± 0.010 μg/ml IC_{50} (A549, 24 h) = 5.3 ± 0.7 μg/ml IC_{50} (A549, 48 h) = 0.279 ± 0.037 μg/ml	[110]
Pegylated folate- and peptide (Pep)-decorated GO GO–Pep–PEG–FA (covalent)	CPT, 90%	HeLa	IC_{50} = 3.1 μM	[111]
GQD–carboxymethyl cellulose (CMC) hydrogel (GQD–CMC)	DOX loading depended on the GQD dose: GQD(10%)–CMC, ~ 4.5%%; GQD(20%)–CMC, ~5.5%%; GQD(30%)–CMC, ~6%	K562	*C* = 2-32 μg/ml IC_{50} (CMC/DOX) = 6.1 μg/ml IC_{50} (GQD 10%/CMC/DOX) = 5.7 μg/ml IC_{50} (GQD 20%/CMC/DOX) = 5.4 μg/ml IC_{50} (GQD 30%/CMC/DOX) = 5.1 μg/ml	[112]
GO–PVP and GO–β-CD	0.17 g of SN-38 per 1 g of GO–PVP; 0.14 g of SN-38 per 1 g of GO–β-CD	MCF-7	IC_{50} (GO–PVP–SN-38) = 97 μM IC_{50} (GO–β-CD–SN-38) = 170 μM	[113]
GO–DOX	DOX, 87%	HEK293 A549 PA-1	IC_{50} (HEK293) = 3.13 μM IC_{50} (A549) = 3.84 μM IC_{50} (PA1) = 3.35 μM IC_{50} (T98G) = 11.80 μM IC_{50} (SK-HEP-1) = 4.11 μM	[114]

Table 1 (*cont.*)

Type of carbon nanoconjugate	Drug load	Cell lines or type of cancer	Applied concentrations and IC_{50} or cytotoxicity (approx. %) at the highest concentration	References
Multifunctional nanocomposite of PEGylated GO with Pt(IV) complex (NGO–PEG–Pt) (*c,c,t*-[$Pt(NH_3)_2Cl_2(OH)_2$])	Pt(IV) content in PEG–NGO–Pt varied from 0.1 to 100 mM, which corresponded to the concentration of NGO–PEG (from 0.89 to 890 mg/ml)	T98G SK-HEP-1 HeLa	IC_{50} (24 h) = 13.88 μM IC_{50} (48 h) = 6.01 μM IC_{50} (72 h) = 3.56 μM	[115]
DOX–loaded aptamer–GO aggregate (GA) (GA–DNA–DOX) DOX–loaded aptamer–GO complex (GC) (GC–DNA–DOX)	DOX, ~10% (wt/wt GO)	HeLa	40% inhibition for dispersion containing 4 μg/ml GA–DNA–DOX (in relation to DOX), 48 h 50% inhibition for dispersion containing 4 μg/ml GC–DNA–DOX (in relation to DOX), 48 h	[116]
GO covalently modified with TNF-related apoptosis-inducing ligand (TRAIL) conjugated with furin-cleavable peptide via PEG linker and noncovalently modified with DOX (fGO–TRAIL–DOX)	DOX, up to 43.8%%	A549	IC_{50} (48 h) = 14 ng/ml (in relation to TRAIL)	[117]
		furin-deficient LoVo cells	IC_{50} (48 h) = 759 ng/ml (in relation to DOX)	
GO covalently modified with TRAIL without furin-cleavable peptide and noncovalently modified with DOX (nGO–TRAIL–DOX)	n/a	A549	IC_{50} = 33 ng/ml (in relation to TRAIL)	[118]
		furin-deficient LoVo cells	IC_{50} = 884 ng/ml (in relation to DOX)	–

Table 2. Application of GBNs in chemotherapy and PTT

GBN	Heat source; energy	Cancer model	References
Spark-generated carboxylic group-activated GO (CGO)-coated hollow mesoporous silica nanoparticles (HMSNs) loaded with topotecan (TPT) (HMSN–NH_2–TPT–CGO); TPT loading, 36 wt. %	NIR irradiation (808 nm); 2.0 W/cm^2, 5 min	MDA-MB-231 (human breast cancer cell line)	[120]
	results: minimal cytotoxicity was observed after treatment with blank nanoparticles; cell viability with HMSN–NH_2–CGO and CGO was ~91 and ~85%, respectively. After NIR irradiation, cell viability after treatment with 200 μg/ml HMSN–NH_2–CGO decreased to ~53%. Cell viability was markedly decreased after treatment with a low dose of HMSN–NH_2–TPT–CGO (after exposure to NIR irradiation), showing its advantage over treatment with free TPT		

Table 2 (*cont.*)

GBN	Heat source; energy	Cancer model	References
GO nanoparticles modified with a conjugate of the photothermal agent IR820 with LA and loaded with DOX; the contents of DOX, IR820-LA, and GO in the GO/DOX/IR820-LA nanohybrids were 22, 42, and 36 wt. %, respectively	NIR (808 nm) or visible (660 nm) irradiation; 1.0 W/cm^2, 5 min	Hep G2/Hep 1-6 (human/murine liver cells)	[121]
	results: both free drug and GO/DOX/IR820-LA nanohybrids exhibited a concentration-dependent antitumor effect. The inhibitory effect of GO/DOX/IR820-LA after laser irradiation was significantly higher than the effects of DOX without laser irradiation and of IR820 and IR820-LA individually after laser irradiation. To evaluate the photothermal capability of the GO/DOX/IR820-LA nanohybrids and IR820 *in vivo*, Hep 1-6 tumor mice were irradiated 6 h after GO/DOX/IR820-LA injection (with saline as a control). In the animals treated with the GO/DOX/IR820-LA nanohybrids, the temperature rose to 52.9°C and the tumor growth was inhibited by 88.0%		
rGO-based nanocomposites functionalized with poly(allylamine hydro-chloride) (rGO–PAH) and loaded with DOX; DOX loading, 36 wt. %	NIR irradiation (808 nm); 6.0 W/cm^2, 20 min	MCF-7	[122]
	results: the nanocomposites demonstrated a highly efficient synergistic chemo-photothermal effect and at a concentration 5 μg/ml caused the death of ~94% MCF-7 cells due to extensive ROS generation, chromosome compression, and DNA disintegration		
Nanohydrogel composed of chondroitin sulphate multiple aldehyde (CSMA), branched polyethylenimine (BPEI) and BPEI-conjugated graphene (BPEI–GO); DOX loading, 60.1 wt. %	NIR irradiation (808 nm); 2.5 W/cm^2, 5 min	MCF-7	[123]
	results: the synergetic chemo-photothermal effect promoted cell death, with 37.8, 22.8, and 9.2% cell survival on days 1, 2, and 3 *in vitro*. In animal treated with the DOX-loaded hydrogel, the cancer recurred ~7 days later than in the animals treated with DOX only, indicating that DOX loading into hydrogels provides sustainable drug release and prolonged cytotoxicity. The combined chemo-photothermal treatment strategy yielded better results, with only two out of six mice (33.3%) developing recurrent cancer		
GO nanoparticles loaded with wedelolactone (WED) and indocyanine green (ICG) on the surface; WED loading, 84.91 wt. %	NIR irradiation (808 nm); 2.0 W/cm^2, 1 min	HeLa	[124]
	results: cell viability in the presence of ICG–Wed–GO after laser irradiation was 12.65%. In treated mice, the tumors reduced gradually and completely disappeared on day 10		
GO nanoparticles functionalized with an amphiphilic polymer based on poly(2-ethyl-2-oxazoline) (POx) and co-loaded with DOX and d-α-tocopherol succinate (TOS); DOX loading, 70 wt. %	NIR irradiation (808 nm); 1.7 W/cm^2, 5 min	MCF-7	[125]
	results: combined application of DOX:TOS-loaded POx–GO and laser irradiation reduced the viability of MCF-7 cells to 39%		
GO nanoparticles conjugated poly(l-lysine) (GO–PLL) deposited on cationic liposomes encapsulating DOX; DOX encapsulation efficiency, 86.4 ± 4.7 wt. %	NIR irradiation (808 nm); 1.5 W/cm^2, 2 min	MDA-MB-231	[126]
	results: MTT and live/dead cellular viability assays suggested that nanoconjugate ensured a dual mode chemotherapy/PTT action. NIR light absorbed by GO and GO–PLL shells was converted to heat and activated the gel leading to the liquid phase transition of the liposomal membrane and release of encapsulated DOX. Alternatively, light absorbed by GO and GO–PLL provided the PTT effect and killed cancer cells (cell viability was less than 20% at the DOX concentration of 5 μg/ml)		

Table 2 (*cont.*)

GBN	Heat source; energy	Cancer model	References
Nanoparticles consisting of histidine (His)-modified amorphous zinc oxide (aZnO) shell on gold nanoparticles (AuNPs) (AuNP–His–aZnO), integrated onto the planar structure of PEGylated GO (PEG–GO); DOX loading, 25 wt. %	NIR irradiation (808 nm); 1.0 W/cm^2, 10 min or 1.5 W/cm^2, 5 min	A549	[127]
	results: the synergetic effect observed at the nanoconjugate concentration of 100 μg/ml upon laser irradiation resulted in almost 100% cell death		
GO nanoparticles coated with FA and AuNPs and loaded with DOX; DOX loading, 72.4 ± 2.5 wt. %	NIR irradiation (808 nm); 0.2 W/cm^2; 5 min or 2.0 W/cm^2; 5 min	MCF-7/HeLa	[128]
	results: the viability of MCF-7 and HeLa cells at the nanoconjugate concentration of 10 μg/ml was 32.5 and 33.9%, respectively. A significant reduction in the tumor volume was observed in mice treated with DOX–GO–AuNPs and DOX–FA–GO–AuNPs (by 27 and 35%, respectively, on day 21). Exposure of mice treated with DOX–GO–AuNPs and DOX–FA–GO–AuNPs to NIR irradiation caused the photothermal effect resulting in even more pronounced tumor reduction to 32 and 43%, respectively, on the 21st day of study		
Nanoplatform consisting of ruthenium nitrosyl functionalized *N*-doped GQDs and a triphenylphosphonium moiety and loaded with nitric oxide (NO)	NIR irradiation (808 nm); 0.6 W/cm^2, 10 min or 1.0 W/cm^2, 10 min	HeLa	[129]
	results: the nanoplatform was fluorescence-trackable and capable of targeting mitochondria in cancer cells. Irradiation of cells led to NO release and photothermal effect, resulting in elimination of tumor cells both *in vitro* (reduction in cell viability to ~10%) and *in vivo* (pronounced inhibition of tumor growth)		
Mesoporous silica (MS)-coated polydopamine-functionalized rGO (prGO) further modified with HA and loaded with DOX; DOX loading, 145 ± 25 wt. %	NIR irradiation (808 nm); 1.5 W/cm^2, 5 min	HeLa	[130]
	results: DOX-loaded prGO–MS–HA nanocomposites produced a significant synergistic chemotherapy/PTT effect upon NIR laser irradiation (cell viability, less than 20%) and strongly suppressed of tumor growth *in vivo*		
GO-hybridised nanogels with alginate loaded with DOX; DOX loading, 97.2 ± 1.2 wt. %	NIR irradiation (808 nm); 4 min	A549	[131]
	results: the antitumor cytotoxicity was enhanced by irradiation with an 808-nm laser (cell viability decreased from 64.0 ± 3.6 to 39.6 ± 5.7%). The temperature of the nanogel aqueous solution increased from 25 to 50°C		
Amino-modified GO (A–GO)	NIR irradiation (808 nm); 6 W/cm^2, 6 min	HSC-3 (oral squamous cell carcinoma cell line)	[132]
	results: *In vitro*, A–GO (15 μg/ml) reduced the viability of HSC-3 cells to 5% upon irradiation (temperature increased to 58.4°C). A–GO strongly reduced the tumor size to 25% of the initial size in 1 out of 4 mice and completely ablated tumors in 3 out of 4 mice		

Table 2 (*cont.*)

GBN	Heat source; energy	Cancer model	References
Dopamine (DOPA)-reduced GO functionalized with sulfobetaine methacrylate (SB) brushes and loaded with IR780 (IR780/SB/DOPA-rGO)	NIR irradiation (808 nm); 1.7 W/cm^2, 10 min	MCF-7	[133]
	results: IR780/SB/DOPA–rGO elicited no cytotoxicity *in vitro* (cell viability, >78%). In contrast, a combination of IR780/SB/DOPA–rGO with NIR light decreased the viability of breast cancer cells to 21%		
DOPA-reduced GO covalently bound with HA and loaded with DOX (DOX/HA–DOPA–rGO); DOX loading, 91.2 wt. %	NIR irradiation (808 nm); 1.7 W/cm^2, 5 min	MCF-7	[134]
	results: a combination of DOX/HA–DOPA–rGO with NIR light reduced cells viability to 23%		
Ultrasmall GO (UGO) (average size, 30 nm) loaded with DOX; DOX loading, 52 wt. %	NIR irradiation (808 nm); 1.5 W/cm^2, 300 s	LO2 (human papillomavirus-related cervical adenocarcinoma cell line)	[94]
	results: a combination of enhanced chemotherapy and PTT induced cell death (cell viability, <15%) in *in vitro* cell tests and suppressed tumor growth in animals		
MTX encapsulated into mesoporous silica nanoparticles (MSNs) by polydopamine (PDA) and embedded into GO nanosheets loaded with naringin (NAR) and cystamine (CYS)	NIR irradiation, 300 min	Saos-2 (osteosarcoma cells)	[135]
	results: in the absence of NIR irradiation, the IC_{50} for NAR/CYS/MTX/MSNs@PDA@GO and MTX/MSNs@PDA@GO were 10.3 and 27.5 mg/ml, respectively. Apparently, a significantly lower IC_{50} of NAR/CYS/MTX/MSNs@PDA@GO was due to the synergistic effect of the two drugs (MTX and NAR). Under NIR irradiation, the IC_{50} of NAR/CYS/MTX/MSNs@PDA@GO decreased further to 3.2 mg/ml, which can be attributed to the synergistic effect of chemotherapy and PTT		

Table 3. The use of GBNs in PDT

Nanomaterial	Conjugated substance	Irradiation characteristics	Cancer model	Result	References
Methylene blue (MB)–GO	MB	red diode radiation	MDA-MB-231	MB–GO (C = 20 mg/ml) reduced cell viability by 80%	[136]
GO–MB/pluronic F127 (PF127)	MB, PF127	LED irradiation at 660 nm	SiHa (squamous cell carcinoma)	GO–MB/PF127 (C = 10 μg/ml) reduced cell viability by 75%	[137]
Pyropheophorbide a (PPa)–NGO– monoclonal antibody against αvβ3 integrin (mAb)	mAb, PPa	laser irradiation at 30 J/cm^2 for 5 min	U-87 MG (human glioblastoma)	PPa–NGO–mAb (C = 1.5 μg/ml) reduced cell viability by 70%	[138]
NGO– methoxy PEG (mPEG)/ zinc phthalocyanine (ZnPc)	ZnPc, mPEG	laser irradiation at 60 J/cm^2 for 5 min	MCF-7	NGO–mPEG/ZnPc (C = 60 mg/l) reduced cell viability by 35%	[139]

Table 3 (*cont.*)

Nanomaterial	Conjugated substance	Irradiation characteristics	Cancer model	Result	References
rGO–ZnO–HA	ZnO, HA	irradiation at 365 nm, 5 mW/cm^2 for 30 min	MDA-MB-231	rGO–ZnO–HA (C = 50 μg/ml) reduced cell viability by 50%	[140]
MB/GQDs and methylene violet (MV)/GQDs	MB or MV	irradiation at 660 nm, 210 mW/cm^2 for 5 min	MCF-7	MB/GQDs and MV/GQDs reduced cell viability by 35% and 10-20%, respectively, at C = 50 μg/ml	[141]
GQDs	GDQs	irradiation at 365 nm up to 5 min	MCF-7 and B16F10 mouse melanoma cells	GQDs reduced viability of MCF-7 and B16F10 cells by more than 90% depending on concentration	[142]
GQDs	GDQs	irradiation at 405 and 637 nm	HeLa	GQDs (C = 1.8 μM) reduced cell viability by 80%	[143]
GO–PEG– chlorin e6 (Ce6)	PEG, Ce6	irradiation at 660 nm, 0.1 W/cm^2 for 10 min	KB (human nasopharyngeal epidermal carcinoma)	GO–PEG–Ce6 (C = 0.011 mg/ml) reduced cell viability by more than 95%	[144]
FA–GO–Ce6	FA, Ce6	irradiation at 632.8 nm with a He-Ne laser for 10 min	MGC803 (human gastric carcinoma)	FA–GO–Ce6 (C = 100 μM) reduced cell viability by 90% (FA–GO to Ce6 ratio, 1 : 1)	[145]
Hypocrellin B (HB)–GO	HB	irradiation at 470 nm with He-Ne laser for 10 min	SMMC-7721 (human hepatocellular carcinoma), SGC-7901 (human gastric cancer cell), HeLa, A549	HB–GO (HB–GO ratio, 1 : 1; C = 5 μM in terms of HB) reduced cell viability by 80 (SMMC-7721), 90 (SGC-7901), 75 (HeLa), and 80%, (A549)	[146]
Upconversion nanoparticles (UCNPs)–NGO/ZnPc	UCNPs, ZnPc, and PEG	irradiation at 630 nm, 60 mW/cm^2 for 10 min	HeLa	UCNPs–NGO/ZnPc (C = 320 μg/ml) reduced cell viability by more than 90%	[147]
GO–PEG–2-(1-hexyloxyethyl)-2-devinylpyropheophorbide-alpha (HPPH)	PEG, HPPH	irradiation at 671 nm, 8 mW/cm^2 for 3 min	4T1 (mouse mammary carcinoma)	GO–PEG–HPPH (C = 1 μM in terms of HPPH) reduced cell viability by more than 80%	[148]
GO–HA–Ce6	HA, Ce6	irradiation at 670 nm, 50 mW/cm^2 for 3 min	A549	GO–HA–Ce6 reduced cell viability by ~80% at C = 1.8 μM (Ce6)	[149]
GO–MB	MB	portable continuous wave diode laser system 655 nm, 150 mW/cm^2	HeLa	GO–MB reduced cell viability by up to 50% at C = 10 μg/ml (GO) and C = 2 μg/ml (MB)	[150]
Hypocrellin A (HcA)/SN-38/GO	HcA, SN-38	irradiation at 470 nm, 25 mW for 5 min	A549	HA/SN-38/GO reduced cell viability by ~95% at C = 6 μM (HA) and C = 6 μM (SN-38)	[151]

Table 3 (*cont.*)

Nanomaterial	Conjugated substance	Irradiation characteristics	Cancer model	Result	References
Magnetic and fluorescent graphene (MFG)–hydrophobic silicon naphthalocyanine *bis*(trihexylsilyl oxide) ($SiNc_4$)	Fluorescent graphene, $SiNc_4$	irradiation at 775 nm, 0.3 W/cm^2 for 60 min	HeLa	MFG–$SiNc_4$ decreased cell viability by ~98% at C = 100 μg/ml	[152]
GO–PEG– sodium sinoporphyrin (DVDMS)	PEG, DVDMS	irradiation at 630 nm, 2 J per well	PC-9 (human non-small cell lung carcinoma)	GO–PEG–DVDMS (C = 3 μg/ml) reduced cell viability by up to 80% (GO–PEG: DVDMS ratio, 1:2)	[153]
p-Nanographene oxide (pGO)–CuS/ICG	copper (II) sulfide, ICG	irradiation at 808 nm, 4 W/cm^2 for 5 min	MCF-7	pGO–CuS/ICG reduced cell viability by ~65% at C = 50 μg/ml	[154]
GO–PEG–DVDMS	PEG, DVDMS	irradiation at 630 nm, radiation dose = 50 J	U-87 MG	GO–PEG–DVDMS (C = 5 μg/ml) reduced cell viability by more than 90%	[155]
ZnPc–PEG–Au@GO nanocolloid (GON) nanoparticles (NPs)	ZnPc, Au, PEG	irradiation at 660 nm, 0.2 W/cm^2 for 10 min	HeLa	ZnPc–PEG–Au@GON NPs (C = 1.2 nM; ZnPc content, $2.8 \cdot 10^{-11}$ M) reduced cell viability by 90%	[156]
GO–808	PEG, branched PEI, heptamethine indocyanine dye IR-808	irradiation at 808 nm, 2 W/cm^2 for 5 min (PTT and PDT)	A549	GO–808 (C = 10 μM in terms of IR-808) led to a reduced cell viability by ~90%	[157]
GO–PEG–FA	PEG, FA	irradiation at 808 nm, 320 mW/cm^2 for 15 min	B16F0 (rat melanoma)	GO–PEG–FA (C = 75 μg/ml) reduced cell viability by 60%	[158]
Hollow magnetic nanospheres (HMNSs) coated with the silica shells and conjugated with carboxylated GQDs, loaded with DOX and stabilized with liposomes (HMNS/SiO_2/GQD-DOX)	HMNSs, liposomes, GQDs, SiO_2, DOX	irradiation at 671 nm for 20 min	Eca-109 (human oesophageal carcinoma)	LP-HMNS/SiO_2/GQD-DOX (C = 0.5 mg/ml for HMNSs, 0.2 mg/ml for GQDs, and 0.3 mg/ml for DOX) decreased cell viability by ~90%	[159]
GO/gold nanostars (AuNSs)–PEG/Ce6	PEG, AuNSs, Ce6	irradiation at 660 nm, 2 W/cm^2 for 15 min	EMT6 (mammary carcinoma cell lines)	GO/AuNS–PEG/Ce6 (C = 3 μg/ml for Ce6, 150 μg/ml for GO/AuNS–PEG) decreased cell viability by up to 80%	[160]
GO–UCNPs–Ce6	UCNPs, Ce6	irradiation at 808 nm for 10 min	HeLa	GO–UCNPs–Ce6 (C = 800 μg/ml) decreased cell viability by up to 85%	[161]

Hence, the developed Pc-graphene nanoplatform has a significant potential as an efficient NIR theranostic probe for imaging and combinatorial phototherapy.

Lamb et al. [165] multifunctionalized graphene nanoflakes (GNFs) with (i) peptide-based Glu–NH–C(O)–NH–Lys ligand capable of binding prostate-specific membrane antigen (PSMA), (ii) potent antimitotic drug (*R*)-Ispinesib, (iii) chelator desferrioxamine B (DFO), and (iv) albumin-binding tag used to extend the half-life of the developed agent *in vivo*. ^{68}Ga-labelled conjugates were used in *in vitro* and *in vivo* experiments to evaluate the performance of GNFs as a theranostic agent (Fig. S5 in the Online Resource 1).

Using the dose-response curves and flow cytometry analysis, it was shown that GNFs loaded with (*R*)-Ispinesib inhibited the kinesin spindle protein (KSP) and induced cell cycle arrest at the G2/M checkpoint. Experiments on the cellular uptake and blocking demonstrated that GNFs functionalized with the Glu–NH–C(O)–NH–Lys ligand showed a specificity toward PSMA-expressing cells (LNCaP cell line). The distribution profile and the excretion rates of ^{68}Ga-labelled GNFs in athymic nude mice were evaluated using the time–activity curves derived by dynamic positron-emission tomography (PET). Imaging experiments showed that GNFs demonstrated low accumulation and retention in background tissues and had a rapid renal clearance.

Tomasella et al. [166] used GO and reduced thiolated GO (rGOSH) as 2D substrates to fabricate nanocomposites with gold nanospheres (AuNSps) or nanorods (AuNRs) via *in situ* reduction of the metal salt precursor and seed-mediated growth processes. The plasmonic sensing capability of the gold-decorated nanosheets was evaluated by UV-visible spectroscopy. *In vitro* experiments on the toxicity of the obtained nanocomposites in human neuroblastoma SH-SY5Y cell indicated a high potential of these hybrids as a plasmonic theranostic platform.

Usman et al. [167] synthesized a bimodal GO-based theranostic nanodelivery system using CA as an anticancer agent, while Gd and AuNPs were used as contrast agents for MRI. CA and Gd were simultaneously loaded on the GO nanolayers via hydrogen bonding and π–π noncovalent interactions to form the GOGCA nanocomposite. Subsequently, AuNPs were doped on the GOGCA surface by means of electrostatic interactions (Fig. S6 in the Online Resource 1). The efficacy (cytotoxicity) of the resulting conjugate was demonstrated in HepG2 hepatocellular carcinoma cells (IC_{50} = 25 μg/ml). At the same time, the conjugate displayed no toxicity toward normal 3T3 fibroblasts. The T1-weighted images of the conjugate obtained by MRI demonstrated contrast enhancement in comparison with the conventional MRI contrast agent $Gd(NO_3)_3$.

Chawda et al. [168] engineered rGO nanoparticles decorated with Gd^{3+} ions. The resulting Gd-containing rGO nanosheets (Gd-rGONSs) were found to enhance the loading of 5-FU (loading capacity, 34%) (Fig. S7 in the Online Resource 1). The drug release was sustained and reached ~92% within 72 h. Gd–rGONSs provided a strong contrast in comparison to the optically responsive bare GO in the swept source optical coherence tomography. The longitudinal relaxivity rate (r_1) for Gd–rGONSs at a magnetic field strength of 1.5 T was 16.85 $mM^{-1}\cdot s^{-1}$, which was four times higher than that of the commercial contrast agent Magnevist (4 $mM^{-1}\cdot s^{-1}$).

Samadian et al. [169] developed a drug delivery nanosystem based on AuNPs, decorated PEG, and FA-conjugated GO. Initially, the graphite powder was oxidised to GO and then functionalized with chloroacetic acid to produce carboxylated graphene oxide (GO–COOH). The obtained GO–COOH was functionalized with the amine end-caped PEG, FA, and 3-amino-1-propanethiol to produce GO–PEG–FA–SH. AuNPs were synthesized through a citrate-mediated reduction and then decorated onto/into GO–PEG–FA–SH through the formation of the Au–S bond to produce the GO–PEG–FA/AuNP nanosystem (Fig. S8 in the Online Resource 1).

The resulting nanosystem was loaded with DOX·HCl (76 wt. %), and its drug-loading capacity and pH-dependent drug release were investigated. The anticancer activity of the developed theranostic agent against MCF-7 cells was evaluated using the MTT assay (IC_{50} = 20 μg/ml after 24 h). This nanomaterial can also be used in the chemotherapy/PTT therapy of solid tumors due to the presence of AuNPs.

Yang et al. [170] developed a biocompatible HA–glutathione (GSH) conjugate (HG) with stabilised gold nanoclusters (AuNCs) combined with GO and loaded with 5-FU (25.3 wt. %) as a novel theranostic platform (HG–AuNC/GO–5-FU) [170]. This multifunctional nanomaterial possessed an excellent fluorescence, photosensitivity, and ability to specifically target cancer cell. Moreover, in the presence of lysosomal hyaluronidase (HAdase) and laser illumination, the recovery of fluorescence and $^1O_2$ and complete release of 5-FU could be achieved, which allows the use HG–AuNC/GO–5-FU in imaging, tumor chemotherapy, hyperthermia treatment, and PDT. This multifunctional complex holds a great potential as a versatile theranostic platform for application in bioimaging-assisted cancer therapy.

Guo et al. [171] double-functionalized GO with FA and Ce6 for combined targeted PTT/PDT against MCF-7 cells and RAW 264.7 macrophages (Fig. S9 in the Online Resource 1). GO–FA/Ce6 exhibited good photothermal properties and high ROS-generating capacity.

This nanomaterial penetrated rapidly into cancer cells via folate receptor-mediated endocytosis, as well as into macrophages. A combination of PTT and PDT allowed to increase the therapeutic efficiency against MCF-7 cancer cells (cell death, up to 65%) compared

to individual treatment. GO–FA/Ce6 also efficiently eliminated RAW 264.7 macrophages due to the effect of PTT/PDT (cell death, up to 94%).

Baktash et al. [172] designed and optimized a hybrid theranostic nanosystem by combining Fe_3O_4 magnetic nanoparticles (MNPs) for imaging and chitosan-grafted GO as a pH-sensitive smart nanocarrier (chitosans with different molecular weights and at different concentrations were used) and investigated the drug (DOX) loading and release properties, biocompatibility, and magnetic characteristics of the developed Fe_3O_4/GO/chitosan nanosystem. It was determined that grafting of the concentrated high-molecular-weight chitosan on MNPs/GO provided efficient drug release and improved DOX loading. Studying the effects of GO and chitosan on the magnetic behavior of the Fe_3O_4/GO system showed that GO decreased the contrast efficiency of the MNPs, while grafting of MNP/GO with hydrophobic chitosan enhanced the contrast, as was seen from a sharp decrease in the r_1 relaxivity, which is very desirable for MRI applications (the r_2/r_1 value for this composite was 28.95, while the r_2/r_1 values for Fe_3O_4/GO and Fe_3O_4 were 6.37 and 14.66, correspondingly). The cytotoxicity assay using L929 cells (normal mouse adipose fibroblasts) revealed a high biocompatibility of the MNP/GO/chitosan nanosystem. Further assays carried out using MNP/GO/chitosan loaded with DOX demonstrated an improved performance of MNP/GO grafted with-low-molecular weight chitosan against MCF-7 cells (cell viability was 39% at 4 μg/ml DOX vs. 53% in the presence of DOX only).

Pan et al. synthesized a covalent conjugate based on GO and silicon phthalocyanine (SiPc) (Fig. S10 in the Online Resource 1) [173].

In vitro studies of the GO–SiPc conjugate in cells showed that this nanomaterial synchronously caused the photothermal effect, intracellular fluorescence, and ROS generation. Efficient photoablation of cancer cells could be triggered by either 671- or 808-nm lasers due to the synergistic PTT/PDT or NIR photothermal effect, respectively. When systemically administered to MCF-7 xenograft mice, GO–SiPc efficiently accumulated at the tumor loci and strongly inhibited tumor growth after laser irradiation.

Chen et al. [174] reported a novel approach to a one-step fabrication of magnetic graphene hybrid nanocomposites GO–PEG–γ-Fe_2O_3 (GPFs) using pulsed laser ablation in liquid method [174]. Due to their good magnetic and photothermal performance, GPFs were employed as nanotheranostic agents for the multimodal imaging-guided chemo/photothermal synergistic therapy. The results of multifunctional *in vivo* imaging confirmed the GPF uptake by the tumors after intravenous injection. Moreover, using the GPF–DOX conjugate allowed to achieve a superior synergistic antitumor effect via combined chemotherapy/PTT. Figure S11 in the Online Resource 1 presents a photograph of hepatocellular carcinoma (H22)-bearing nude mice under different treatments (Fig. S12 in the Online Resource 1 demonstrates the difference in the relative tumor volume after the treatment).

A multifunctional theranostic nanoplatform based on GO and $MnWO_4$ was developed by *in situ* growth of $MnWO_4$ nanoparticles onto GO surfaces in a PEG-containing hyperthermia polyol medium [175]. In comparison with GO and $MnWO_4$/PEG, the NIR absorbance of the GO/$MnWO_4$/PEG nanocomposite was significantly improved, resulting in an enhanced photothermal conversion capability and good photoacoustic (PA) imaging performance. In addition, the longitudinal relaxivity r_1 of GO/$MnWO_4$/PEG reached 11.34 $mM^{-1}\cdot s^{-1}$ in a 0.5-T magnetic field, which was significantly higher than for ordinary Mn(II)-based T1 agents. *In vivo* MRI and PA imaging studies demonstrated that GO/$MnWO_4$/PEG could be used as an efficient bimodal contrast agent to guide cancer treatment. GO/$MnWO_4$/PEG showed a high loading capacity for DOX (550 mg/g); the resulting conjugate demonstrated a pronounced cytotoxic activity towards 4T1 (human breast carcinoma) and HUVEC (human umbilical vein endothelial cells) cell lines. For example, cells incubated with 100 μg/ml GO/$MnWO_4$/PEG/DOX (containing 5 μg/ml DOX) and then exposed to laser irradiation showed the highest mortality rate (about 90%) vs. 50% in the case of DOX (C = 5 μg/ml) or GO/$MnWO_4$/PEG.

Prasad et al. [176] reported the results of *in vivo* photo-triggered tumor regression induced by application of a biodegradable red emissive nanotheranostic composite based on liposomes fortified with GO flakes and functionalized with FA (GO–Lipo–FA) and loaded with DOX (Fig. S13 in the Online Resource 1) [176].

The synthesized nanocomposite has a good aqueous dispersibility, quick photothermal response (54°C in 5 min), high biocompatibility, deep intracellular localization, feasibility for 4T1 visualisation, and long-term tumor-binding ability of the injected emissive nanohybrid. GO enhanced the stability of the drug-loaded liposomes in the extracellular environment, which prevented premature release of the loaded anticancer drug from the liposomal cavity. In addition, the authors demonstrated the developed nanocomposite caused tumor regression (~300 to 25 mm^3) in 4T1 Balb/c mice.

Foroushani et al. [177] developed a theranostic system based on GO integrated with PDA, BSA, diethylenetriaminepentaacetic acid (DTPA)–Mn(II) contrast agent, FA, and 5-FU for targeting CT-26 colon cancer cells via folate receptors overexpressed on cancer cells. According to the results of biodistribution assessment, the conjugate was observed mainly in the tumors and, therefore, provided highly efficient drug delivery to CT-26 cells. *In vitro* and *in vivo* MRI and therapy examination confirmed the ability of the conjugate

to enhance the contrast in tumor imaging (diagnostics) and to inhibit the growth of cancer cells (therapy).

Luo et al. [178] proposed an easy method for the synthesis of a theranostic agent based on superparamagnetic iron oxide nanoparticles loaded onto GO nanosheets (SPIONs@GO) and cis-aconitic anhydride-DOX prodrug (CAD) attached to the carboxylic groups of GO through the 2-poly(amidoamine) dendrimer (G2.NH2) linker (Fig. S14 in the Online Resource 1).

The release of DOX from the conjugate was pH-sensitive: 66.91 ± 3.16% at pH 5.5 and 47.51 ± 1.87% at pH 6.5 within 12 h. The viability of 4T1 cells after treatment with CAD–SPIONs@GO for 24 h decreased cell viability from 93.8% to 38.3% at the DOX concentration of 1.3-20 μM (similar to the treatment with free DOX). According to the results of biodistribution experiments, 4 h after injection, CAD–SPIONs@GO mainly localized to the spleen and liver. The total Fe amount in all major organs decreased greatly 12 h after injection, suggesting that CAD–SPIONs@GO was cleared out of the body. The authors proposed that the interface effect between GO and *in situ* growth of SPIONs contributed to the significant increase in the r_1 value and decrease in the r_2 value. *In vivo* studies results confirmed a possibility of conjugate application in high-resolution T1-weighted MRI.

Shi et al. [179] synthesized a theranostic agent based on rGO conjugated to the anti-CD105 antibody (TRC105) and a complex of ^{64}Cu (PET label; half-life, 12.7 h) with 1,4,7-triazacyclononane-1,4,7-triacetic acid (NOTA, chelator). *In vivo* experiments on the blockade of the agent uptake by 4T1 cells with an excess of TRC105, as well as flow cytometry and histology data, confirmed the stability of ^{64}Cu–NOTA–rGO–TRC105 and its specificity for CD105 of the tumor vasculature. Noteworthy, ^{64}Cu–NOTA–RGO–TRC105 exhibited little extravasation in 4T1 cells, indicating that targeting tumor vasculature (instead of tumor cell) can be a valid and preferred approach for the application of nanomaterials. Since rGO can be used for PTT, the tumor-specific rGO conjugate may serve as a promising theranostic agent that integrates imaging and therapeutic components.

Cheng et al. [180] developed a mild thermal annealing procedure to induce blue fluorescence in GO suspensions (Fig. S15 in the Online Resource 1) [180]. The procedure preserved the oxygen functional groups, which enabled conjugation of a cancer drug and resulted in nontoxic and harmless nanomaterial. The authors demonstrated the capability of GO to simultaneously act as a cellular imaging agent and a drug delivery agent in CT26 cancer cells without the need for additional fluorescent protein labelling. The authors also covalently annealed GO with CP (elemental content of Pt in the conjugate, ~3 wt. %) and determined that the annealed GO boosted the therapeutic performance of CP in killing CT26 cancer cells.

Hu et al. [181] synthesized a new conjugate based on rGO, PDA, and ICG for amplifying the PA imaging and PTT effects for cancer phototheranostic (Fig. S16 in the Online Resource 1). The procedure for the ICG–PDA–rGO preparation included the following steps: (i) dopamine monomers were loaded on the GO surface and spontaneously self-polymerised via the Michael addition/Schiff reaction to form a PDA coating on the rGO surface, (ii) free ICG dye was absorbed on the PDA–rGO surface via hydrogen bonds and π–π stacking interactions.

ICG–PDA–rGO exhibited stronger PTT effect and higher PA contrast than pure GO and PDA–rGO. After PA imaging-guided PTT treatment, the tumors in 4T1 breast subcutaneous and orthotopic mice models were suppressed completely; no treatment-induced toxicity was observed.

Turcheniuk et al. [182] produced a theranostic agent based on AuNRs coated with pegylated rGO (AuNRs@rGO–PEG) and modified with sulfo-cyanine7 fluorescent dye (Cy7) and Tat protein (see Fig. S17 in the Online Resource 1).

Selective targeting of tumors was ensured by specific interaction between the Tat protein and human glioblastoma astrocytoma cells (U87MG). Due to the presence of NIR fluorescent dye integrated onto the rGO shell, the conjugate acted as fluorescent cellular marker. *In vivo* experiments in mice implanted with U87MG cells showed that irradiation at 800 nm (0.7 W/cm^2, 10 min) suppressed tumor growth after 5 days. Histological analysis of tumor tissues revealed an active uptake of the nanoparticles by the tumor stromal cells and selective damage of tumor vessels.

Wang et al. [183] synthesized a novel nanomaterial for the PTT/immunotherapy of cancer by the self-assembly of oleate-capped Fe_3O_4 nanoparticles (FNPs) and rGO through electrostatic interaction, followed by modification with PEG–NH_2 [182]. FNP/rGO–PEG nanocomposites can be used for the MRI-guided cancer PTT/immunotherapy due to their excellent magnetic properties. Under laser irradiation (805 nm), FNP/rGO–PEG improved the PTT efficacy by increasing the temperature up to 60°C and killing 80% of 4T1 orthotopic mouse breast tumor cells. In addition, FNP/rGO–PEG nanocomposites could be used to stimulate immune response by triggering the maturation of dendritic cells ($CD11c^+$ $CD86^+$) and secretion of cytokines (IL-12p70, IL-6). Intratumoral injection of FNP/rGO–PEG nanocomposites in combination with NIR laser irradiation significantly increased the median survival time of tumor-bearing animals.

Bansal et al. [184] developed a theranostic agent based on GQDs conjugated with a biosurfactant isolated from *Candida parapsilosis* through the amine-carboxyl coupling reaction and noncovalent modification with FA. The obtained conjugate had a homogenous

dispersion and showed the photoluminescence properties and demonstrated enhanced uptake by cancerous cells in comparison with non-modified GQDs. In the MTT assay, the conjugate decreased the viability of MCF-7 cells by more than 60% after 24 h of incubation and by 75% after 48 h [184].

Ko et al. [185] synthesized GQDs for the diagnostics and therapy of breast cancer via conjugation with two precursors. DOX-disulfide-GQDs provided chemotherapy and PEG-disulfide-herceptin enhanced the half-life and ensured the targeting of HER2 (Fig. S18 in the Online Resource 1) [184]. The cleavage of disulfide links at a physiologically relevant glutathione concentration in cancer cells provided controlled drug release. The authors demonstrated an enhanced cellular uptake of the conjugate by SK-BR-3 cells (HER2-positive) in comparison with MDA-MB-231 cells (HER2-negative). As a result, the viability of SK-BR-3 cells was significantly decreased (to <50%) at the conjugate concentration of 50 mg/ml, whereas the viability of MDA-MB-231 cells was reduced to >85%.

Iannazzo et al. [9] developed a novel conjugate based on GQDs covalently modified with the tumor targeting module biotin (BTN) and noncovalently modified with DOX (GQD-BTN-DOX, Fig. S19 in the Online Resource 1), as well as the GQD-DOX conjugate [9]. The DOX content in GQD-BTN-DOX and GQD-DOX was 16.6 and 17.8 wt. %, respectively. GQD-DOX nanoparticles were preferentially accumulated in the cytoplasm, while DOX localized to the nuclei. At the same time, GQD-BTN-DOX nanoparticles concentrated in the endosomal compartment after endocytosis-mediated internalisation. The cytotoxicity of GQD-BTN-DOX towards A549 cells strongly depended on the uptake by the cells, which was more pronounced and delayed for GQD-BTN-DOX in comparison with GQD-DOX and DOX only.

Li et al. [186] synthesized a covalent GQD-FA conjugate and loaded it with IR780 iodide (33.19 wt. %) via π–π stacking interactions (see Fig. S20 in the Online Resource 1). *In vivo* NIR fluorescence imaging and biodistribution analysis demonstrated that in BALB/c nude mice xenografted with HeLa cells, the conjugate preferentially accumulated in the tumors. When irradiated with an 808-nm laser, IR780/GQDs-FA caused hyperthermia (photothermal conversion efficiency, 87.9%) and induced apoptosis of cancer cells and tumor necrosis, resulting in complete tumor disappearance without relapse.

Ding et al. [187] developed a novel type of GQD-based theranostic agent with a superior therapeutic performance against 4T1 cancer cells both in *in vitro* [IC_{50} (theranostic agent) = 1.5 g/ml, IC_{50} (DOX) = 4 g/ml] and *in vivo* (the conjugate reduced the tumor volume 2.7 times more than DOX alone) due to the improved tissue penetration and cellular uptake [187]. GQDs were synthesized via facile chemical oxidation and exfoliation technique using polyacrylonitrile carbon fibres as a raw material. The NIR fluorescent molecule Cy5.5 was covalently attached to GQDs via the cathepsin D-responsive peptide (Phe-Ala-Ala-Phe-Phe-Val-Leu-Cys, P); functionalized GQDs were then loaded with DOX via π–π interactions. The synthesized construct allowed to track the delivery and release of the anticancer drug, as well as to monitor drug-induced apoptosis of cancer cells through GQD, DOX, and Cy5.5 characteristic fluorescence.

Badrigilan et al. [188] produced a theranostic agent based on superparamagnetic iron oxide and bismuth (III) oxide (Bi_2O_3) with GQDs for *in vitro* computed tomography (CT)/MR dual-mode bioimaging and PTT (Fig. S21 in the Online Resource 1).

The GQD-Fe/Bi nanocomposite had the following advantages: (i) the photothermal conversion efficacy was 31.8% with a high photostability upon irradiation with a NIR 808-nm laser; (ii) photothermal ablation of HeLa and MCF-7 cells *in vitro* resulted in a significant decrease in cell viability (~50% at 100 μg/ml) in comparison with laser treatment only (3.0%); (iii) obtained nanoparticles exhibited a superior X-ray attenuation capability (175%) in comparison with Dotarem (macrocyclic gadolinium-based contrast agent), as well as showed a strong T2-relaxation shortening capability (r_2 = 62.34 $mM^{-1}\cdot s^{-1}$) as a contrast agent for CT/MRI.

The same authors synthesized GQD-coated bismuth nanoparticles and assessed the possibility of their application for CT imaging and PTT [189].

Lee et al. [190] developed rGQDs derived by rGO top-down oxidation and HA-GQDs (HGQDs) that were hydrothermally synthesized by the bottom-up method [190]. The obtained nanomaterials possessed substantial NIR absorption and fluorescence throughout the visible and NIR regions, which is beneficial for *in vivo* imaging. Aqueous dispersions of rGQDs and HGQDs added to HeLa cells and irradiated with NIR laser (λ = 808 nm, 0.9 W/cm^2, 10 min) facilitated an increase in temperature up to 54.5°C, leading to the decrease in the HeLa cell viability from 80% for RGQDs (C = 1.5 mg/ml) and 60% for HGQDs (C = 1.7 mg/ml) without irradiation down to ~40% (RGQDs) and ~20% (HGQDs) after irradiation.

Sung et al. [191] synthesized a unique conjugate composed of porous carbon/silica nanosponge encapsulated with GQDs loaded with docetaxel (DTX) via π–π interactions; then, the particles were capped with the red blood cell (RBC) membrane and cetuximab via fusion (see Fig. S22 in the Online Resource 1).

The obtained conjugate has the following advantages: (i) the stability of the RBC lipids and proteins on porous particles was higher than that of lipids of liposomal particles due to a high adhesion energy; (ii) the porous surface of the particles exhibited an excellent lateral bilayer fluidity, thus improving the

targeting efficacy; (iii) RBC-coated nanoparticles had a considerably longer circulation time than PEGylated nanoparticles due to the presence of transmembrane protein CD47 that induces signalling through the phagocyte receptor CD172a, inhibits immune response, and suppresses particle recognition by the immune system (see Fig. S23 in the Online Resource 1 for the mechanism of conjugate action).

Due to the synergistic effect of biomimetic targeting and penetration of DTX/GQD nanoparticles followed by irradiation (1.5 W/cm^2, 10 min), it was able to achieve a significant reduction in the size of A549 tumor during the first 10 days of treatment.

Xuan et al. [192] synthesized nanoparticles for bioimaging and combined chemotherapy/PTT based on AuNSp clusters (diameter of 50 nm) coated with GQDs covalently modified by FA using carbodiimide method and noncovalently modified with DOX (94.39 ± 0.39%) (see Fig. S24 in the Online Resource 1 for the scheme of conjugate synthesis).

The obtained nanoparticles formed stable aqueous dispersions and demonstrated an excellent PA and CT imaging performance, low cytotoxicity, and PTT conversion efficiency up to 51.31%. In addition, the authors showed a significant decrease in the relative tumor volume in BALB/c nude mice (SPF males, 4-week-old) inoculated with HeLa cells (Fig. S25 in the Online Resource 1).

Wu et al. [193] developed a new type of theranostic agent named PC@GCpD(Gd) [192]. First, the authors synthesized GQDs covalently modified with the Ce6 photosensitiser (GCpD) and coated with PDA layers, yielding water-compatible and biocompatible nanoparticles with a substantial photothermal/photochemical effect. Then, the Cy3-labelled nonmethylated CpG oligodeoxynucleotide (5′-TCC ATG ACG TTC CTG ACG TT-3′-Cy3) was condensed with the biodegradable cationic poly(l-lysine) (PLL) polypeptide to obtain immunoactive nanoparticles (PCs). GCpD nanocomposites easily self-assembled on the surface of PC nanoimmunocores and then were chelated with Gd^{3+} (see Fig. S26 in the Online Resource 1).

The obtained photo/immunoactive hybrid PC@GCpD(Gd) nanostructures decreased the viability of cancer cells, released endogenous cancer cell antigens, and contemporaneously regulated tumor microenvironment to facilitate the immunostimulatory effect. The authors characterised the cellular uptake, MRI/fluorescence imaging, and phototherapeutic and immunostimulatory activity towards the murine mammary cancer EMT6 model, as well as the biosafety of PC@GCpD(Gd) nanoparticles. It was shown that laser irradiation (660 nm, 1 W/cm^2, 10 min) simulated the PTT and PDT effects, leading to a significant decrease in the EMT6 cell viability in mice, secretion of proinflammatory cytokines, maturation of dendritic cells, and recruitment of $CD4^+$ and $CD8^+$ T cells into the tumor, resulting in a higher therapeutic efficacy. MRI/fluorescence imaging traced specific accumulation and retention of PC@GCpD(Gd) in the tumor-draining lymph nodes.

Ruiyi et al. [194] synthesized histidine (His)- and octadecylamine (OA)-functionalized GQDs (His/OA-GQDs). The obtained nanoparticles were used for the fabrication of His/OA-GQD-$NaYF_4$:Yb,Tm nanocages that exhibited a 140.2-fold enhancement of upconversion fluorescence, stability in aqueous solutions, and high DOX-loading capacity (461.2% within 30 min) (see Fig. S27 in the Online Resource 1) [194]. The authors also developed a drug delivery system (GYAuDOX) which included His/OA-GQD-$NaYF_4$:Yb,Tm gold nanoparticles as a core, and MGC-803 cell membrane as a shell. The obtained material exhibited a high biocompatibility, selective targeting of homotypic tumor cells, pH- and light-stimulated DOX release, and capacity for chemotherapy/PTT. The data on the efficacy of the obtained theranostic agent are presented in Fig. S28 in the Online Resource 1.

Liu et al. [195] synthesized GQDs with a strong absorption (1070 nm) in the NIR-II region (1000-1700 nm) by a one-step solvothermal treatment using phenol (carbon precursor) and hydrogen peroxide (oxidising agent) in the magnetic field with an intensity of 9 T (see Fig. S29 in the Online Resource 1) [195].

The synthesized nanoparticles possessed a uniform size (3.6 nm), tunable fluorescence (quantum yield, 16.67%), and high photothermal conversion efficacy (33.45%). The obtained nanomaterial ablated tumor cells, inhibited tumor growth upon NIR-II irradiation, and, at the same time, provided an enhanced NIR imaging of tumors in mice.

Zhang et al. [196] developed a nanomaterial (named R-NCNP) by coating a mesoporous carbon nitride (C_3N_4) layer on a core–shell nitrogen-doped GQD (N-GQD)@ HMSNs and decorated it with a P-PEG-RGD polymer consisting of a purified hematoporphyrin derivative photofrin (P) and the tumor-homing peptide RGD (Arg-Gly-Asp) connected by PEG as a linker, to achieve the targeted delivery (see Fig. S30 in the Online Resource 1).

The obtained material has the following advantages for biomedicine applications: (i) R-NCNPs catalyzed water decomposition in the tumor microenvironment with the generation of oxygen, thus decreasing local hypoxia; (ii) the generated oxygen bubbles enhanced generation of an echogenic signal, making them laser-activatable ultrasound imaging agents; (iii) activation of the encapsulated photosensitisers and C_3N_4-layered photosensitiser at λ = 630 nm stimulated ROS formation; (iv) combination of PTT with PDT for tumor eradication; (v) P-PEG-RGD promoted efficient accumulation of particles in the tumor; (vi) R-NCNPs acted as multimodal real-time monitoring agent.

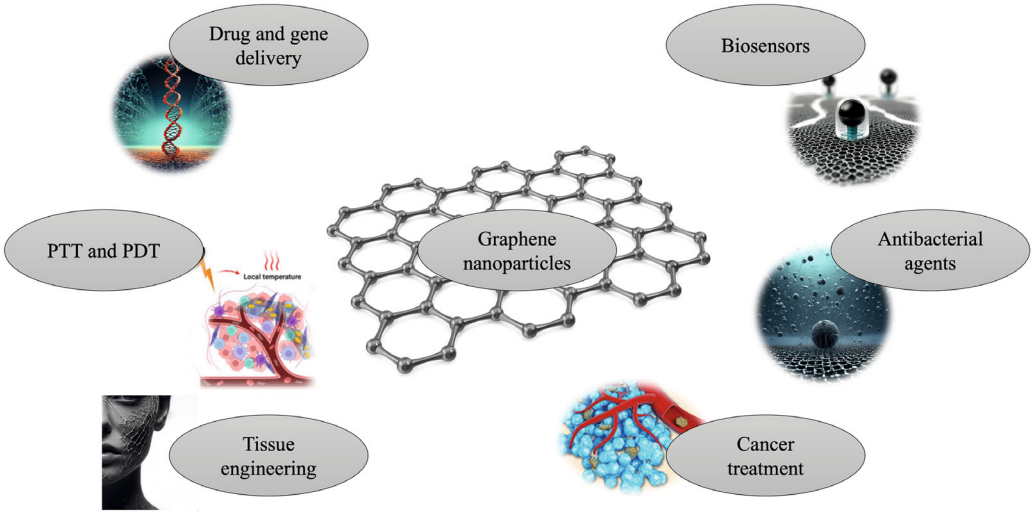

Fig. 8. Directions of GBN scientific applications.

Prasad et al. [197] synthesized a theranostic agent based on GQD-embedded mesoporous silica which displayed a high penetration and retention ability in solid tumors (see Fig. S31 in the Online Resource 1). The obtained material had a uniform particle size distribution, improved stability, high surface area (850 m^2/g), DOX loading capacity of 31%, and high photothermal response. It was shown that administration of carbanosilica in 4T1 female Balb/c mice led to a temperature rise (to ~55°C after 5 min of exposure to NIR light), fluorescence intensity of 10^8 $p/s/cm^2/sr$, and as a result, provided 68.75% tumor shrinking compared to 34.48% without NIR irradiation.

Yang et al. [198] developed a self-assembly approach to the theranostic agent synthesis based on the acidity-activated GQD nanotransformers (GQD NTs) by mixing (i) GQDs (loading module) that provided large surface area for the loading of photosensitiser [*tetrakis*(4-carboxylphenyl) porphyrin, TCPP] and MRI contrast agent (Mn-TCPP), (ii) RGD peptide as a targeting module due to its affinity to $\alpha_V\beta_3$ integrin, and (iii) linking module that connected the first two modules through the host–guest interactions between β-CD and adamantine [198]. As seen from Fig. S32 in the Online Resource 1, the acidity of tumor microenvironment triggered GQD NT transformation and drugs release.

The synthesized theranostic agent provided an efficient targeting and long-term retention in the tumor (over 96 h), possibility of MRI/fluorescence imaging, and photothermal effect, which enhanced cell membrane permeability, as well as an efficient photosensitiser uptake and repeated PDT at a photosensitiser content 10-30 times lower than in previously published papers. As seen from Fig. S33 in the Online Resource 1 (survival and tumor growth curves of A549 tumor-bearing mice after different treatments), the developed nanomaterial significantly inhibited tumor growth and increased mouse survival.

CONCLUSION

Since their discovery in 2004, graphene and its derivatives have become some of the most promising materials due to a broad range of potential applications in various fields of science and technology, such as biotechnology, biomedicine, tissue engineering, bioanalysis, etc. (Fig. 8).

Graphene has a unique two-dimensional flat structure, unique physical and chemical properties, and high biocompatibility, which promotes its application in the creation of high-tech materials for biomedical purposes. The use of graphene and its derivatives for the treatment of solid tumors is one of the promising areas of modern oncology. Along with the advantages of GBNs, there are also some limitations that need to be considered. One of the main problems is the lack of information about metabolic pathways and toxicokinetics of graphene materials used in biomedical applications. This limits the ability to fully evaluate the safety and efficacy of these materials in living organisms. Another important problem is poor reproducibility of the synthesis of graphene-based materials and common lack of comprehensive studies on their structure and composition. Both these factors lead to a poor reproducibility of biological effects of graphene-based materials in living systems. Also, water dispersions of GBNs are prone to aggregation, which affects their biological activity and mechanism of biological action. In this regard, it is necessary to conduct a comprehensive physico-chemical investigation of their stability, including the studies of optimal stabilizers. Let us hope that these problems will be solved in the XXI century – the century of nanotechnology.

Supplementary information. The online version contains supplementary material available at https://doi.org/10.1134/S0006297924080029.

Contributions. K.N.S., I.V.M., J.A.R., and V.V.S. created the study concept; K.N.S., I.V.M., J.A.R., and V.V.S. developed the study methodology; K.N.S., D.N.M., D.K.K., J.A.R., O.E.M., and V.V.S. supervised the study; V.V.S., D.N.M., O.E.M., and K.N.S. acquired the funding; O.S.S., S.V.A., G.O.I., and P.K.K. investigated and analyzed the data; K.N.S., P.A.A., and V.V.S. curated the data; O.S.S. wrote the draft and prepared the figures; K.N.S., S.V.A., and V.V.S. reviewed and edited the manuscript.

Funding. The work was carried out with the financial support of the Ministry of Health of the Russian Federation (state assignment on the topic "Creation of a drug based on nanoforms of innovative synthetic antitumor antibiotics, including heterocyclic systems with a quaternized nitrogen atom and styryl fragments in the form of conjugates with targeted delivery vectors to the tumor microenvironment" EGISU: 1023022200055-4-3.2.21;3.1.3).

Ethics declarations. This work does not contain any studies involving human and animal subjects. The authors of this work declare that they have no conflicts of interest.

REFERENCES

1. Shin, S. R., Li, Y. C., Jang, H. L., Khoshakhlagh, P., Akbari, M., Nasajpour, A., Zhang, Y. S., Tamayol, A., and Khademhosseini, A. (2016) Graphene-based materials for tissue engineering, *Adv. Drug Deliv. Rev.*, **105**, 255-274, https://doi.org/10.1016/j.addr.2016.03.007.
2. Lin, J., Huang, Y., and Huang, P. (2018) Graphene-Based Nanomaterials in Bioimaging, in *Biomedical Applications of Functionalized Nanomaterials: Concepts, Development and Clinical Translation*, Elsevier, pp. 247-287, https://doi.org/10.1016/b978-0-323-50878-0.00009-4.
3. Feng, L. L., Wu, Y. X., Zhang, D. L., Hu, X. X., Zhang, J., Wang, P., Song, Z. L., Zhang, X. B., and Tan, W. (2017) Near infrared graphene quantum dots-based two-photon nanoprobe for direct bioimaging of endogenous ascorbic acid in living cells, *Anal. Chem.*, **89**, 4077-4084, https://doi.org/10.1021/acs.analchem.6b04943.
4. Thapa, R. K., Kim, J. H., Jeong, J. H., Shin, B. S., Choi, H. G., Yong, C. S., and Kim, J. O. (2017) Silver nanoparticle-embedded graphene oxide-methotrexate for targeted cancer treatment, *Colloids Surf. B Biointerfaces*, **153**, 95-103, https://doi.org/10.1016/j.colsurfb.2017.02.012.
5. Zhang, C., Liu, Z., Zheng, Y., Geng, Y., Han, C., Shi, Y., Sun, H., Zhang, C., Chen, Y., Zhang, L., Guo, Q., Yang, L., Zhou, X., and Kong, L. (2018) Glycyrrhetinic acid functionalized graphene oxide for mitochondria targeting and cancer treatment *in vivo*, *Small*, **14**, 1703306, https://doi.org/10.1002/smll.201703306.
6. Liu, J., Dong, J., Zhang, T., and Peng, Q. (2018) Graphene-based nanomaterials and their potentials in advanced drug delivery and cancer therapy, *J. Controll. Rel.*, **286**, 64-73, https://doi.org/10.1016/j.jconrel.2018.07.034.
7. Yang, K., Feng, L., and Liu, Z. (2016) Stimuli responsive drug delivery systems based on nano-graphene for cancer therapy, *Adv. Drug Deliv. Rev.*, **105**, 228-241, https://doi.org/10.1016/j.addr.2016.05.015.
8. Fan, H., Yu, X., Wang, K., Yin, Y., Tang, Y., Tang, Y., and Liang, X. (2019) Graphene quantum dots (GQDs)-based nanomaterials for improving photodynamic therapy in cancer treatment, *Eur. J. Med. Chem.*, **182**, 111620, https://doi.org/10.1016/j.ejmech.2019.111620.
9. Iannazzo, D., Pistone, A., Salamò, M., Galvagno, S., Romeo, R., Giofré, S. V., Branca, C., Visalli, G., and Di Pietro, A. (2017) Graphene quantum dots for cancer targeted drug delivery, *Int. J. Pharm.*, **518**, 185-192, https://doi.org/10.1016/j.ijpharm.2016.12.060.
10. Hai, X., Feng, J., Chen, X., and Wang, J. (2018) Tuning the optical properties of graphene quantum dots for biosensing and bioimaging, *J. Mater. Chem. B*, **6**, 3219-3234, https://doi.org/10.1039/c8tb00428e.
11. Szunerits, S., and Boukherroub, R. (2018) Graphene-based biosensors, *Interf. Focus*, **8**, 20160132, https://doi.org/10.1098/rsfs.2016.0132.
12. Peña-Bahamonde, J., Nguyen, H. N., Fanourakis, S. K., and Rodrigues, D. F. (2018) Recent advances in graphene-based biosensor technology with applications in life sciences, *J. Nanobiotechnol.*, **16**, 75, https://doi.org/10.1186/s12951-018-0400-z.
13. Palmieri, V., and Papi, M. (2020) Can graphene take part in the fight against COVID-19? *Nano Today*, **33**, 100883, https://doi.org/10.1016/j.nantod.2020.100883.
14. Yang, X. X., Li, C. M., Li, Y. F., Wang, J., and Huang, C. Z. (2017) Synergistic antiviral effect of curcumin functionalized graphene oxide against respiratory syncytial virus infection, *Nanoscale*, **9**, 16086-16092, https://doi.org/10.1039/c7nr06520e.
15. Chen, Y.-N., Hsueh, Y.-H., Hsieh, C.-T., Tzou, D.-Y., and Chang, P.-L. (2016) Antiviral activity of graphene-silver nanocomposites against non-enveloped and en-

veloped viruses, *Int. J. Environ. Res. Public Health*, **13**, 430, https://doi.org/10.3390/ijerph13040430.

16. Du, T., Lu, J., Liu, L., Dong, N., Fang, L., Xiao, S., and Han, H. (2018) Antiviral activity of graphene oxide-silver nanocomposites by preventing viral entry and activation of the antiviral innate immune response, *ACS Appl. Bio Mater.*, **1**, 1286-1293, https://doi.org/10.1021/acsabm.8b00154.
17. Shi, L., Chen, J., Teng, L., Wang, L., Zhu, G., Liu, S., Luo, Z., Shi, X., Wang, Y., and Ren, L. (2016) The antibacterial applications of graphene and its derivatives, *Small*, **12**, 4165-4184, https://doi.org/10.1002/smll.201601841.
18. Ji, H., Sun, H., and Qu, X. (2016) Antibacterial applications of graphene-based nanomaterials: recent achievements and challenges, *Adv. Drug Deliv. Rev.*, **105**, 176-189, https://doi.org/10.1016/j.addr.2016.04.009.
19. Xia, M. Y., Xie, Y., Yu, C. H., Chen, G. Y., Li, Y. H., Zhang, T., and Peng, Q. (2019) Graphene-based nanomaterials: the promising active agents for antibiotics-independent antibacterial applications, *J. Controll. Rel.*, **307**, 16-31, https://doi.org/10.1016/j.jconrel.2019.06.011.
20. Kumar, P., Huo, P., Zhang, R., and Liu, B. (2019) Antibacterial properties of graphene-based nanomaterials, *Nanomaterials*, **9**, 737, https://doi.org/10.3390/nano9050737.
21. Wu, X., Li, H., and Xiao, N. (2018) Advancement of Near-infrared (NIR) laser interceded surface enactment of proline functionalized graphene oxide with silver nanoparticles for proficient antibacterial, antifungal and wound recuperating therapy in nursing care in hospitals, *J. Photochem. Photobiol. B*, **187**, 89-95, https://doi.org/10.1016/j.jphotobiol.2018.07.015.
22. Kahsay, M. H., Belachew, N., Tadesse, A., and Basavaiah, K. (2020) Magnetite nanoparticle decorated reduced graphene oxide for adsorptive removal of crystal violet and antifungal activities, *RSC Adv.*, **10**, 34916-34927, https://doi.org/10.1039/d0ra07061k.
23. Hermanová, S., Zarevúcká, M., Bouša, D., Pumera, M., and Sofer, Z. (2015) Graphene oxide immobilized enzymes show high thermal and solvent stability, *Nanoscale*, **7**, 5852-5858, https://doi.org/10.1039/c5nr00438a.
24. Li, H., Fierens, K., Zhang, Z., Vanparijs, N., Schuijs, M. J., Van Steendam, K., Feiner Gracia, N., De Rycke, R., De Beer, T., De Beuckelaer, A., De Koker, S., Deforce, D., Albertazzi, L., Grooten, J., Lambrecht, B. N., and De Geest, B. G. (2016) Spontaneous protein adsorption on graphene oxide nanosheets allowing efficient intracellular vaccine protein delivery, *ACS Appl. Mater. Interfaces*, **8**, 1147-1155, https://doi.org/10.1021/acsami.5b08963.
25. Kavitha, T., Kang, I. K., and Park, S. Y. (2014) Poly(acrylic acid)-grafted graphene oxide as an intracellular protein carrier, *Langmuir*, **30**, 402-409, https://doi.org/10.1021/la404337d.
26. Emadi, F., Amini, A., Gholami, A., and Ghasemi, Y. (2017) Functionalized graphene oxide with chitosan for protein nanocarriers to protect against enzymatic cleavage and retain collagenase activity, *Sci. Rep.*, **7**, 42258, https://doi.org/10.1038/srep42258.
27. Zhao, H., Ding, R., Zhao, X., Li, Y., Qu, L., Pei, H., Yildirimer, L., et al. (2017) Graphene-based nanomaterials for drug and/or gene delivery, bioimaging, and tissue engineering, *Drug Discov. Today*, **22**, 1302-1317, https://doi.org/10.1016/j.drudis.2017.04.002.
28. Paul, A., Hasan, A., Kindi, H. A., Gaharwar, A. K., Rao, V. T. S., Nikkhah, M., Shin, S. R., Krafft, D., Dokmeci, M. R., Shum-Tim, D., and Khademhosseini, A. (2014) Injectable graphene oxide/hydrogel-based angiogenic gene delivery system for vasculogenesis and cardiac repair, *ACS Nano*, **8**, 8050-8062, https://doi.org/10.1021/nn5020787.
29. Chen, B., Liu, M., Zhang, L., Huang, J., Yao, J., and Zhang, Z. (2011) Polyethylenimine-functionalized graphene oxide as an efficient gene delivery vector, *J. Mater. Chem.*, **21**, 7736-7741, https://doi.org/10.1039/c1jm10341e.
30. Imani, R., Shao, W., Taherkhani, S., Emami, S. H., Prakash, S., and Faghihi, S. (2016) Dual-functionalized graphene oxide for enhanced siRNA delivery to breast cancer cells, *Colloids Surf. B Biointerfaces*, **147**, 315-325, https://doi.org/10.1016/j.colsurfb.2016.08.015.
31. Yue, H., Zhou, X., Cheng, M., and Xing, D. (2018) Graphene oxide-mediated Cas9/sgRNA delivery for efficient genome editing, *Nanoscale*, **10**, 1063-1071, https://doi.org/10.1039/c7nr07999k.
32. Tang, Z., Wu, H., Cort, J. R., Buchko, G. W., Zhang, Y., Shao, Y., Aksay, I. A., Liu, J., and Lin, Y. (2010) Constraint of DNA on functionalized graphene improves its biostability and specificity, *Small*, **6**, 1205-1209, https://doi.org/10.1002/smll.201000024.
33. Lu, C. H., Zhu, C. L., Li, J., Liu, J. J., Chen, X., and Yang, H. H. (2010) Using graphene to protect DNA from cleavage during cellular delivery, *Chem. Commun.*, **46**, 3116-3118, https://doi.org/10.1039/b926893f.
34. Park, J., and Yan, M. (2013) Covalent functionalization of graphene with reactive intermediates, *Acc Chem Res*, **46**, 181-189, https://doi.org/10.1021/ar300172h.
35. Criado, A., Melchionna, M., Marchesan, S., and Prato, M. (2015) The covalent functionalization of graphene on substrates, *Angewandte Chemie Int. Edn.*, **54**, 10734-10750, https://doi.org/10.1002/anie.201501473.
36. Georgakilas, V., Tiwari, J. N., Kemp, K. C., Perman, J. A., Bourlinos, A. B., et al. (2016) Noncovalent functionalization of graphene and graphene oxide for energy materials, biosensing, catalytic, and biomedical applications, *Chem. Rev.*, **116**, 5464-5519, https://doi.org/10.1021/acs.chemrev.5b00620.
37. Georgakilas, V., Otyepka, M., Bourlinos, A. B., Chandra, V., Kim, N., Kemp, K. C., Hobza, P., Zboril, R., and Kim, K. S. (2012) Functionalization of graphene:

Covalent and non-covalent approaches, derivatives and applications, *Chem. Rev.*, **112**, 6156-6214, https://doi.org/10.1021/cr3000412.
38. Wei, D., Liu, Y., Wang, Y., Zhang, H., Huang, L., and Yu, G. (2009) Synthesis of n-doped graphene by chemical vapor deposition and its electrical properties, *Nano Lett.*, **9**, 1752-1758, https://doi.org/10.1021/nl803279t.
39. Sreeprasad, T. S., and Berry, V. (2013) How do the electrical properties of graphene change with its functionalization? *Small*, **9**, 341-350, https://doi.org/10.1002/smll.201202196.
40. Falkovsky, L. A. (2008) Optical properties of graphene, *J. Phys. Conf. Ser.*, **129**, 12004, https://doi.org/10.1088/1742-6596/129/1/012004.
41. Qiu, B., Zhao, X. W., Hu, G. C., Yue, W. W., Yuan, X. B., and Ren, J. F. (2020) Tuning optical properties of Graphene/WSe2 heterostructure by introducing vacancy: first principles calculations, *Physica E Low Dimens Syst. Nanostruct.*, **116**, 113729, https://doi.org/10.1016/j.physe.2019.113729.
42. Kumar, A., Sharma, K., and Dixit, A. R. (2020) A review on the mechanical and thermal properties of graphene and graphene-based polymer nanocomposites: understanding of modelling and MD simulation, *Mol. Simul.*, **46**, 136-154, https://doi.org/10.1080/08927022.2019.1680844.
43. Aradhana, R., Mohanty, S., and Nayak, S. K. (2018) Comparison of mechanical, electrical and thermal properties in graphene oxide and reduced graphene oxide filled epoxy nanocomposite adhesives, *Polymer (Guildf)*, **141**, 109-123, https://doi.org/10.1016/j.polymer.2018.03.005.
44. Vu, T. V., Hieu, N. V., Phuc, H. V., Hieu, N. N., Bui, H. D., Idrees, M., Amin, B., and Nguyen, C. V. (2020) Graphene/WSeTe van der Waals heterostructure: Controllable electronic properties and Schottky barrier via interlayer coupling and electric field, *Appl. Surf. Sci.*, **507**, 145036, https://doi.org/10.1016/j.apsusc.2019.145036.
45. Wang, Q., Li, X., Wu, L., Lu, P., and Di, Z. (2019) Electronic and interface properties in graphene oxide/hydrogen-passivated Ge heterostructure, *Rapid Res. Lett.*, **13**, 1800461, https://doi.org/10.1002/pssr.201800461.
46. Sang, M., Shin, J., Kim, K., and Yu, K. (2019) Electronic and thermal properties of graphene and recent advances in graphene based electronics applications, *Nanomaterials*, **9**, 374, https://doi.org/10.3390/nano9030374.
47. Papageorgiou, D. G., Kinloch, I. A., and Young, R. J. (2017) Mechanical properties of graphene and graphene-based nanocomposites, *Prog. Mater. Sci.*, **90**, 75-127, https://doi.org/10.1016/j.pmatsci.2017.07.004.
48. Zhao, X., Zhang, Q., Chen, D., and Lu, P. (2010) Enhanced mechanical properties of graphene-based polyvinyl alcohol composites, *Macromolecules*, **43**, 2357-2363, https://doi.org/10.1021/ma902862u.
49. Geim, A. K., and Novoselov, K. S. (2007) The rise of graphene, *Nat. Mater.*, **6**, 183-191, https://doi.org/10.1038/nmat1849.
50. Lee, H. C., Liu, W.-W., Chai, S.-P., Mohamed, A. R., Lai, C. W., Khe, C.-S., Voon, C. H., Hashim, U., and Hidayah, N. M. S. (2016) Synthesis of single-layer graphene: a review of recent development, *Procedia Chem.*, **19**, 916-921, https://doi.org/10.1016/j.proche.2016.03.135.
51. Adetayo, A., and Runsewe, D. (2019) Synthesis and fabrication of graphene and graphene oxide: a review, *Open J. Composite Mater.*, **09**, 207-229, https://doi.org/10.4236/ojcm.2019.92012.
52. Zhang, Y., Zhang, L., and Zhou, C. (2013) Review of chemical vapor deposition of graphene and related applications, *Acc. Chem. Res.*, **46**, 2329-2339, https://doi.org/10.1021/ar300203n.
53. Muñoz, R., and Gómez-Aleixandre, C. (2013) Review of CVD synthesis of graphene, *Chem. Vapor Deposition*, **19**, 297-322, https://doi.org/10.1002/cvde.201300051.
54. Li, X., Colombo, L., and Ruoff, R. S. (2016) Synthesis of graphene films on copper foils by chemical vapor deposition, *Adv. Mater.*, **28**, 6247-6252, https://doi.org/10.1002/adma.201504760.
55. Chen, K., Shi, L., Zhang, Y., and Liu, Z. (2018) Scalable chemical-vapour-deposition growth of three-dimensional graphene materials towards energy-related applications, *Chem. Soc. Rev.*, **47**, 3018-3036, https://doi.org/10.1039/c7cs00852j.
56. Yang, X., Zhang, G., Prakash, J., Chen, Z., Gauthier, M., and Sun, S. (2019) Chemical vapour deposition of graphene: layer control, the transfer process, characterisation, and related applications, *Int. Rev. Phys. Chem.*, **38**, 149-199, https://doi.org/10.1080/0144235x.2019.1634319.
57. Mattevi, C., Kim, H., and Chhowalla, M. (2011) A review of chemical vapour deposition of graphene on copper, *J. Mater. Chem.*, **21**, 3324-3334, https://doi.org/10.1039/c0jm02126a.
58. Zhou, H., Yu, W. J., Liu, L., Cheng, R., Chen, Y., Huang, X., Liu, Y., Wang, Y., Huang, Y., and Duan, X. (2013) Chemical vapour deposition growth of large single crystals of monolayer and bilayer graphene, *Nat. Commun.*, **4**, 2096, https://doi.org/10.1038/ncomms3096.
59. Yu, P., Lowe, S. E., Simon, G. P., and Zhong, Y. L. (2015) Electrochemical exfoliation of graphite and production of functional graphene, *Curr. Opin. Colloid Interface Sci.*, **20**, 329-338, https://doi.org/10.1016/j.cocis.2015.10.007.
60. Rao, K. S., Senthilnathan, J., Liu, Y. F., and Yoshimura, M. (2014) Role of peroxide ions in formation of graphene nanosheets by electrochemical exfoliation of graphite, *Sci. Rep.*, **4**, 4237, https://doi.org/10.1038/srep04237.
61. Wan, H., Wei, C., Zhu, K., Zhang, Y., Gong, C., et al. (2017) Preparation of graphene sheets by electrochemical exfoliation of graphite in confined space and their application in transparent conductive films, *ACS Appl. Mater.*

Interfaces, **9**, 34456-34466, https://doi.org/10.1021/acsami.7b09891.

62. Mir, A., and Shukla, A. (2018) Bilayer-rich graphene suspension from electrochemical exfoliation of graphite, *Mater Des.*, **156**, 62-70, https://doi.org/10.1016/j.matdes.2018.06.035.
63. Melezhik, A. V., Pershin, V. F., Memetov, N. R., and Tkachev, A. G. (2016) Mechanochemical synthesis of graphene nanoplatelets from expanded graphite compound, *Nanotechnol. Russ.*, **11**, 421-429, https://doi.org/10.1134/s1995078016040121.
64. Guex, L. G., Sacchi, B., Peuvot, K. F., Andersson, R. L., Pourrahimi, A. M., Ström, V., Farris, S., and Olsson, R. T. (2017) Experimental review: chemical reduction of graphene oxide (GO) to reduced graphene oxide (rGO) by aqueous chemistry, *Nanoscale*, **9**, 9562-9571, https://doi.org/10.1039/c7nr02943h.
65. De Silva, K. K. H., Huang, H. H., Joshi, R. K., and Yoshimura, M. (2017) Chemical reduction of graphene oxide using green reductants, *Carbon N Y*, **119**, 190-199, https://doi.org/10.1016/j.carbon.2017.04.025.
66. Wang, J., Salihi, E. C., and Šiller, L. (2017) Green reduction of graphene oxide using alanine, *Mater. Sci. Engin. C*, **72**, 1-6, https://doi.org/10.1016/j.msec.2016.11.017.
67. Alam, S. N., Sharma, N., and Kumar, L. (2017) Synthesis of graphene oxide (GO) by modified hummers method and its thermal reduction to obtain reduced graphene oxide (rGO)*, *Graphene*, **6**, 1-18, https://doi.org/10.4236/graphene.2017.61001.
68. Saleem, H., Haneef, M., and Abbasi, H. Y. (2018) Synthesis route of reduced graphene oxide via thermal reduction of chemically exfoliated graphene oxide, *Mater. Chem. Phys.*, **204**, 1-7, https://doi.org/10.1016/j.matchemphys.2017.10.020.
69. Oliveira, A. E. F., Braga, G. B., Tarley, C. R. T., and Pereira, A. C. (2018) Thermally reduced graphene oxide: synthesis, studies and characterization, *J. Mater. Sci.*, **53**, 12005-12015, https://doi.org/10.1007/s10853-018-2473-3.
70. Schedy, A., and Oetken, M. (2020) The thermal reduction of graphene oxide – a simple and exciting manufacturing process of graphene, *CHEMKON*, **27**, 244-249, https://doi.org/10.1002/ckon.201900049.
71. Abdelhalim, A. O. E., Sharoyko, V. V., Meshcheriakov, A. A., Martynova, S. D., Ageev, S. V., Iurev, G. O., Al Mulla, H., Petrov, A. V., Solovtsova, I. L., Vasina, L. V., Murin, I. V., and Semenov, K. N. (2020) Reduction and functionalization of graphene oxide with L-cysteine: synthesis, characterization and biocompatibility, *Nanomedicine*, **29**, 102284, https://doi.org/10.1016/j.nano.2020.102284.
72. Kaplan, A., Yuan, Z., Benck, J. D., Govind Rajan, A., Chu, X. S., Wang, Q. H., and Strano, M. S. (2017) Current and future directions in electron transfer chemistry of graphene, *Chem. Soc. Rev.*, **46**, 4530-4571, https://doi.org/10.1039/c7cs00181a.
73. Sturala, J., Luxa, J., Pumera, M., and Sofer, Z. (2018) Frontispiece: chemistry of graphene derivatives: synthesis, applications, and perspectives, *Chem. Eur. J.*, **24**, 5992-6006, https://doi.org/10.1002/chem.201704192.
74. Gao, W. (2015) The chemistry of graphene oxide, in *Graphene Oxide: Reduction Recipes, Spectroscopy, and Applications*, Springer International Publishing, pp. 61-95, https://doi.org/10.1007/978-3-319-15500-5_3.
75. Banks, C. E., Vedyagin, A. A., Cui, Y., Liu, L., Shi, M., Wang, Y., Meng, X., Chen, Y., Huang, Q., and Liu, C. (2024) A review of advances in graphene quantum dots: from preparation and modification methods to application, *J. Carbon. Res.*, **10**, 7, https://doi.org/10.3390/c10010007.
76. Prakash, S. H., and Roopan, S. M. (2023) A comprehensive review on recent developments in the graphene quantum dot framework for organic transformations, *J. Organomet. Chem.*, **997**, 122790, https://doi.org/10.1016/j.jorganchem.2023.122790.
77. Gozali Balkanloo, P., Mohammad Sharifi, K., and Poursattar Marjani, A. (2023) Graphene quantum dots: synthesis, characterization, and application in wastewater treatment: a review, *Mater. Adv.*, **4**, 4272-4293, https://doi.org/10.1039/d3ma00372h.
78. Thangadurai, T. D., Manjubaashini, N., Nataraj, D., Gomes, V., and Lee, Y. I. (2022) A review on graphene quantum dots, an emerging luminescent carbon nanolights: healthcare and environmental applications, *Mater. Sci. Engin. B*, **278**, 115633, https://doi.org/10.1016/j.mseb.2022.115633.
79. Kadyan, P., Malik, R., Bhatia, S., Al Harrasi, A., Mohan, S., Yadav, M., Dalal, S., Ramniwas, S., Kumar Kataria, S., and Arasu, T. (2023) Comprehensive review on synthesis, applications, and challenges of graphene quantum dots (GQDs), *J. Nanomater.*, **2023**, 2832964, https://doi.org/10.1155/2023/2832964.
80. Ghaffarkhah, A., Hosseini, E., Kamkar, M., Sehat, A. A., Dordanihaghighi, S., Allahbakhsh, A., Van Der Kuur, C., Arjmand, M., Ghaffarkhah, A., Hosseini, E., Kamkar, M., Sehat, A. A., Dordanihaghighi, S., Arjmand, M., and Allahbakhsh, A. (2022) Synthesis, applications, and prospects of graphene quantum dots: a comprehensive review, *Small*, **18**, 2102683, https://doi.org/10.1002/smll.202102683.
81. Zhao, C., Song, X., Liu, Y., Fu, Y., Ye, L., et al. (2020) Synthesis of graphene quantum dots and their applications in drug delivery, *J. Nanobiotechnol.*, **18**, 142, https://doi.org/10.1186/s12951-020-00698-z.
82. Pinto, A. M., Moreira, J. A., Magalhães, F. D., and Gonçalves, I. C. (2016) Polymer surface adsorption as a strategy to improve the biocompatibility of graphene nanoplatelets, *Colloids Surf. B Biointerfaces*, **146**, 818-824, https://doi.org/10.1016/j.colsurfb.2016.07.031.
83. Abdelhalim, A. O. E., Meshcheriakov, A. A., Maistrenko, D. N., Molchanov, O. E., Ageev, S. V., Ivanova, D. A., Iamalova, N. R., Luttsev, M. D., Vasina, L. V.,

Sharoyko, V. V., and Semenov, K. N. (2021) Graphene oxide enriched with oxygen-containing groups: on the way to an increase of antioxidant activity and biocompatibility, *Colloids Surf. B Biointerfaces*, **210**, 112232, https://doi.org/10.1016/j.colsurfb.2021.112232.

84. Galebskaya, L. V., Solovtsova, I. L., Miroshnikova, E. B., Mikhailova, I. A., Sushkin, M. E., Razumny, A. V., Babina, A. V., and Fomina, V. A. (2017) The importance of a photosensitizer bleaching registration for the evaluation of mechanism of preparation action on the photo-induced hemolysis, *Biomed. Photonics*, **6**, 33-38, https://doi.org/10.24931/2413-9432-2017-6-3-33-38.
85. Abdelhalim, A. O. E., Sharoyko, V. V., Meshcheriakov, A. A., Luttsev, M. D., Potanin, A. A., Iamalova, N. R., Zakharov, E. E., Ageev, S. V., Petrov, A. V., Vasina, L. V., Solovtsova, I. L., Nashchekin, A. V., Murin, I. V., and Semenov, K. N. (2020) Synthesis, characterisation and biocompatibility of graphene-L-methionine nanomaterial, *J. Mol. Liq.*, **314**, 113605, https://doi.org/10.1016/j.molliq.2020.113605.
86. Abdelhalim, A. O. E., Sharoyko, V. V., Ageev, S. V., Farafonov, V. S., Nerukh, D. A., Postnov, V. N., Petrov, A. V., and Semenov, K. N. (2021) Graphene oxide of extra high oxidation: a wafer for loading guest molecules, *J. Phys. Chem. Lett.*, **12**, 10015-10024, https://doi.org/10.1021/acs.jpclett.1c02766.
87. Sharoyko, V. V., Shemchuk, O. S., Meshcheriakov, A. A., Andoskin, P. A., Petrov, A. V., Rumyantsev, A. M., Sambuk, E. V., Maystrenko, D. N., Molchanov, O. E., Murin, I. V., Charykov, N. A., and Semenov, K. N. (2024) Modification of fullerene with amino acids as a method for obtaining biocompatible materials with a protective effect, *Fullerenes Nanotubes Carbon Nanostructures*, **32**, 631-639, https://doi.org/10.1080/1536383x.2023.2291484.
88. Ageev, S. V., Semenov, K. N., Shemchuk, O. S., Iurev, G. O., Andoskin, P. A., Rumiantsev, A. M., Sambuk, E. V., Kozhukhov, P. K., Maistrenko, D. N., Molchanov, O. E., Murin, I. V., Mazur, A. S., and Sharoyko, V. V. (2024) Synthesis, biocompatibility and biological activity of a graphene oxide-folic acid conjugate for cytarabine delivery, *Colloids Surf. A Physicochem. Eng. Asp.*, **697**, 134360, https://doi.org/10.1016/j.colsurfa.2024.134360.
89. Singh, S. K., Singh, M. K., Kulkarni, P. P., Sonkar, V. K., Grácio, J. J. A., and Dash, D. (2012) Amine-modified graphene: thrombo-protective safer alternative to graphene oxide for biomedical applications, *ACS Nano*, **6**, 2731-2740, https://doi.org/10.1021/nn300172t.
90. Podolska, M. J., Barras, A., Alexiou, C., Frey, B., Gaipl, U., Boukherroub, R., Szunerits, S., Janko, C., and Muñoz, L. E. (2020) Graphene oxide nanosheets for localized hyperthermia – physicochemical characterization, biocompatibility, and induction of tumor cell death, *Cells*, **9**, 776, https://doi.org/10.3390/cells9030776.
91. Ding, Z., Ma, H., and Chen, Y. (2014) Interaction of graphene oxide with human serum albumin and its mechanism, *RSC Adv.*, **4**, 55290-55295, https://doi.org/10.1039/c4ra09613d.
92. Taneva, S. G., Krumova, S., Bogár, F., Kincses, A., Stoichev, S., Todinova, S., Danailova, A., Horváth, J., Násztor, Z., Kelemen, L., and Dér, A. (2021) Insights into graphene oxide interaction with human serum albumin in isolated state and in blood plasma, *Int. J. Biol. Macromol.*, **175**, 19-29, https://doi.org/10.1016/j.ijbiomac.2021.01.151.
93. Feng, L., Zhang, S., and Liu, Z. (2011) Graphene based gene transfection, *Nanoscale*, **3**, 1252, https://doi.org/10.1039/c0nr00680g.
94. Li, X., Wang, Y., Liu, T., Zhang, Y., Wang, C., and Xie, B. (2023) Ultrasmall graphene oxide for combination of enhanced chemotherapy and photothermal therapy of breast cancer, *Colloids Surf. B Biointerfaces*, **225**, 113288, https://doi.org/10.1016/j.colsurfb.2023.113288.
95. Akhavan, O., Ghaderi, E., and Akhavan, A. (2012) Size-dependent genotoxicity of graphene nanoplatelets in human stem cells, *Biomaterials*, **33**, 8017-8025, https://doi.org/10.1016/j.biomaterials.2012.07.040.
96. Sharoyko, V. V., Mikolaichuk, O. V., Shemchuk, O. S., Abdelhalim, A. O. E., Potanin, A. A., Luttsev, M. D., Dadadzhanov, D. R., Vartanyan, T. A., Petrov, A. V., Shasherina, A. Yu., Murin, I. V., Maistrenko, D. N., Molchanov, O. E., and Semenov, K. N. (2023) Novel non-covalent conjugate based on graphene oxide and alkylating agent from 1,3,5-triazine class, *J. Mol. Liq.*, **372**, 121203, https://doi.org/10.1016/j.molliq.2023.121203.
97. Yang, Q., Wang, X., Chen, J., Tian, C., Li, H., Chen, Y., and Lv, Q. (2012) A clinical study on regional lymphatic chemotherapy using an activated carbon nanoparticle-epirubicin in patients with breast cancer, *Tumor Biol.*, **33**, 2341-2348, https://doi.org/10.1007/s13277-012-0496-y.
98. Sun, X., Liu, Z., Welsher, K., Robinson, J. T., Goodwin, A., Zaric, S., and Dai, H. (2008) Nano-graphene oxide for cellular imaging and drug delivery, *Nano Res.*, **1**, 203-212, https://doi.org/10.1007/s12274-008-8021-8.
99. Wu, J., Wang, Y. S., Yang, X. Y., Liu, Y. Y., Yang, J. R., Yang, R., and Zhang, N. (2012) Graphene oxide used as a carrier for adriamycin can reverse drug resistance in breast cancer cells, *Nanotechnology*, **23**, 355101, https://doi.org/10.1088/0957-4484/23/35/355101.
100. Fan, X., Jiao, G., Gao, L., Jin, P., and Li, X. (2013) The preparation and drug delivery of a graphene-carbon nanotube-Fe 3O4 nanoparticle hybrid, *J. Mater. Chem. B*, **1**, 2658-2664, https://doi.org/10.1039/c3tb00493g.
101. Zhang, L., Lu, Z., Zhao, Q., Huang, J., Shen, H., and Zhang, Z. (2011) Enhanced chemotherapy efficacy by sequential delivery of siRNA and anticancer drugs using PEI-grafted graphene oxide, *Small*, **7**, 460-464, https://doi.org/10.1002/smll.201001522.

102. Liu, Z., Robinson, J. T., Sun, X., and Dai, H. (2008) PEGylated nanographene oxide for delivery of water-insoluble cancer drugs, *J. Am. Chem. Soc.*, **130**, 10876-10877, https://doi.org/10.1021/ja803688x.
103. Zhang, L., Xia, J., Zhao, Q., Liu, L., and Zhang, Z. (2010) Functional graphene oxide as a nanocarrier for controlled loading and targeted delivery of mixed anticancer drugs, *Small*, **6**, 537-544, https://doi.org/10.1002/smll.200901680.
104. Xu, Q., Wang, H., Gu, W., Xiao, N., and Ye, L. (2014) Chlorotoxin-conjugated graphene oxide for targeted delivery of an anticancer drug, *Int. J. Nanomedicine*, **9**, 1433, https://doi.org/10.2147/ijn.s58783.
105. Fan, L., Ge, H., Zou, S., Xiao, Y., Wen, H., Li, Y., Feng, H., and Nie, M. (2016) Sodium alginate conjugated graphene oxide as a new carrier for drug delivery system, *Int. J. Biol. Macromol.*, **93**, 582-590, https://doi.org/10.1016/j.ijbiomac.2016.09.026.
106. Rosli, N. F., Fojtů, M., Fisher, A. C., and Pumera, M. (2019) Graphene oxide nanoplatelets potentiate anticancer effect of cisplatin in human lung cancer cells, *Langmuir*, **35**, 3176-3182, https://doi.org/10.1021/acs.langmuir.8b03086.
107. Deb, A., and Vimala, R. (2018) Camptothecin loaded graphene oxide nanoparticle functionalized with polyethylene glycol and folic acid for anticancer drug delivery, *J. Drug Deliv. Sci. Technol.*, **43**, 333-342, https://doi.org/10.1016/j.jddst.2017.10.025.
108. Pooresmaeil, M., and Namazi, H. (2018) β-Cyclodextrin grafted magnetic graphene oxide applicable as cancer drug delivery agent: synthesis and characterization, *Mater. Chem. Phys.*, **218**, 62-69, https://doi.org/10.1016/j.matchemphys.2018.07.022.
109. Bullo, S., Buskaran, K., Baby, R., Dorniani, D., Fakurazi, S., and Hussein, M. Z. (2019) Dual drugs anticancer nanoformulation using graphene oxide-PEG as nanocarrier for protocatechuic acid and chlorogenic acid, *Pharm. Res.*, **36**, 91, https://doi.org/10.1007/s11095-019-2621-8.
110. Ma, N., Liu, J., He, W., Li, Z., Luan, Y., Song, Y., and Garg, S. (2017) Folic acid-grafted bovine serum albumin decorated graphene oxide: an efficient drug carrier for targeted cancer therapy, *J. Colloid Interface Sci.*, **490**, 598-607, https://doi.org/10.1016/j.jcis.2016.11.097.
111. Tian, J., Luo, Y., Huang, L., Feng, Y., Ju, H., and Yu, B. Y. (2016) Pegylated folate and peptide-decorated graphene oxide nanovehicle for *in vivo* targeted delivery of anticancer drugs and therapeutic self-monitoring, *Biosens. Bioelectron.*, **80**, 519-524, https://doi.org/10.1016/j.bios.2016.02.018.
112. Javanbakht, S., and Namazi, H. (2018) Doxorubicin loaded carboxymethyl cellulose/graphene quantum dot nanocomposite hydrogel films as a potential anticancer drug delivery system, *Mater. Sci. Engin. C*, **87**, 50-59, https://doi.org/10.1016/j.msec.2018.02.010.
113. Karki, N., Tiwari, H., Pal, M., Chaurasia, A., Bal, R., Joshi, P., and Sahoo, N. G. (2018) Functionalized graphene oxides for drug loading, release and delivery of poorly water soluble anticancer drug: a comparative study, *Colloids Surf. B Biointerfaces*, **169**, 265-272, https://doi.org/10.1016/j.colsurfb.2018.05.022.
114. Abdelhalim, A. O. E., Ageev, S. V., Petrov, A. V., Meshcheriakov, A. A., Luttsev, M. D., Vasina, L. V., Nashchekina, I. A., Murin, I. V., Molchanov, O. E., Maistrenko, D. N., Potanin, A. A., Semenov, K. N., and Sharoyko, V. V. (2022) Graphene oxide conjugated with doxorubicin: synthesis, bioactivity, and biosafety, *J. Mol. Liq.*, **359**, 119156, https://doi.org/10.1016/j.molliq.2022.119156.
115. Li, J., Lyv, Z., Li, Y., Liu, H., Wang, J., Zhan, W., Chen, H., Chen, H., and Li, X. (2015) A theranostic prodrug delivery system based on Pt(IV) conjugated nano-graphene oxide with synergistic effect to enhance the therapeutic efficacy of Pt drug, *Biomaterials*, **51**, 12-21, https://doi.org/10.1016/j.biomaterials.2015.01.074.
116. Mo, R., Jiang, T., Sun, W., and Gu, Z. (2015) ATP-responsive DNA-graphene hybrid nanoaggregates for anticancer drug delivery, *Biomaterials*, **50**, 67-74, https://doi.org/10.1016/j.biomaterials.2015.01.053.
117. Jiang, T., Sun, W., Zhu, Q., Burns, N. A., Khan, S. A., Mo, R., and Gu, Z. (2015) Furin-mediated sequential delivery of anticancer cytokine and small-molecule drug shuttled by graphene, *Adv. Mater.*, **27**, 1021-1028, https://doi.org/10.1002/adma.201404498.
118. Mehra, N. K., Jain, A. K., and Nahar, M. (2018) Carbon nanomaterials in oncology: an expanding horizon, *Drug Discov Today*, **23**, 1016-1025, https://doi.org/10.1016/j.drudis.2017.09.013.
119. Jiang, B., Zhou, B., Lin, Z., Liang, H., and Shen, X. (2019) Recent advances in carbon nanomaterials for cancer phototherapy, *Chem. Eur. J.*, **25**, 3993-4004, https://doi.org/10.1002/chem.201804383.
120. Gautam, M., Thapa, R. K., Poudel, B. K., Gupta, B., Ruttala, H. B., Nguyen, H. T., Soe, Z. C., Ou, W., Poudel, K., Choi, H.-G., Ku, S. K., Yong, C. S., and Kim, J. O. (2019) Aerosol technique-based carbon-encapsulated hollow mesoporous silica nanoparticles for synergistic chemo-photothermal therapy, *Acta Biomater.*, **88**, 448-461, https://doi.org/10.1016/j.actbio.2019.02.029.
121. Huang, C., Hu, X., Hou, Z., Ji, J., Li, Z., and Luan, Y. (2019) Tailored graphene oxide-doxorubicin nanovehicles via near-infrared dye-lactobionic acid conjugates for chemo-photothermal therapy, *J. Colloid Interface Sci.*, **545**, 172-183, https://doi.org/10.1016/j.jcis.2019.03.019.
122. Roy, S., Sarkar, A., and Jaiswal, A. (2019) Poly(allylamine hydrochloride)-functionalized reduced graphene oxide for synergistic chemo-photothermal therapy, *Nanomedicine*, **14**, 255-274, https://doi.org/10.2217/nnm-2018-0320.
123. Li, Q., Wen, J., Liu, C., Jia, Y., Wu, Y., Shan, Y., Qian, Z., and Liao, J. (2019) Graphene-nanoparticle-based

self-healing hydrogel in preventing postoperative recurrence of breast cancer, *ACS Biomater. Sci. Eng.*, **5**, 768-779, https://doi.org/10.1021/acsbiomaterials.8b01475.

124. Zhang, X., Luo, L., Li, L., He, Y., Cao, W., Liu, H., Niu, K., and Gao, D. (2019) Trimodal synergistic antitumor drug delivery system based on graphene oxide, *Nanomedicine*, **15**, 142-152, https://doi.org/10.1016/j.nano.2018.09.008.
125. De Melo-Diogo, D., Costa, E. C., Alves, C. G., Lima-Sousa, R., Ferreira, P., Louro, R. O., and Correia, I. J. (2018) POxylated graphene oxide nanomaterials for combination chemo-phototherapy of breast cancer cells, *Eur. J. Pharmaceut. Biopharmaceut.*, **131**, 162-169, https://doi.org/10.1016/j.ejpb.2018.08.008.
126. Hashemi, M., Omidi, M., Muralidharan, B., Tayebi, L., Herpin, M. J., Mohagheghi, M. A., Mohammadi, J., Smyth, H. D. C., and Milner, T. E. (2018) Layer-by-layer assembly of graphene oxide on thermosensitive liposomes for photo-chemotherapy, *Acta Biomater.*, **65**, 376-392, https://doi.org/10.1016/j.actbio.2017.10.040.
127. Zhang, M., Wu, F., Wang, W., Shen, J., Zhou, N., and Wu, C. (2019) Multifunctional nanocomposites for targeted, photothermal, and chemotherapy, *Chem. Mater.*, **31**, 1847-1859, https://doi.org/10.1021/acs.chemmater.8b00934.
128. Chauhan, G., Chopra, V., Tyagi, A., Rath, G., Sharma, R. K., and Goyal, A. K. (2017) "Gold nanoparticles composite-folic acid conjugated graphene oxide nanohybrids" for targeted chemo-thermal cancer ablation: *in vitro* screening and *in vivo* studies, *Eur. J. Pharmaceut. Sci.*, **96**, 351-361, https://doi.org/10.1016/j.ejps.2016.10.011.
129. Guo, M., Xiang, H.-J., Wang, Y., Zhang, Q.-L., An, L., Yang, S.-P., Ma, Y., Wang, Y., and Liu, J.-G. (2017) Ruthenium nitrosyl functionalized graphene quantum dots as an efficient nanoplatform for NIR-light-controlled and mitochondria-targeted delivery of nitric oxide combined with photothermal therapy, *Chem. Commun.*, **53**, 3253-3256, https://doi.org/10.1039/c7cc00670e.
130. Shao, L., Zhang, R., Lu, J., Zhao, C., Deng, X., and Wu, Y. (2017) Mesoporous silica coated polydopamine functionalized reduced graphene oxide for synergistic targeted chemo-photothermal therapy, *ACS Appl. Mater. Interfaces*, **9**, 1226-1236, https://doi.org/10.1021/acsami.6b11209.
131. Xu, X., Wang, J., Wang, Y., Zhao, L., Li, Y., and Liu, C. (2018) Formation of graphene oxide-hybridized nanogels for combinative anticancer therapy, *Nanomedicine*, **14**, 2387-2395, https://doi.org/10.1016/j.nano.2017.05.007.
132. Chen, G., Yang, Z., Yu, X., Yu, C., Sui, S., Zhang, C., Bao, C., Zeng, X., Chen, Q., and Peng, Q. (2023) Intratumor delivery of amino-modified graphene oxide as a multifunctional photothermal agent for efficient antitumor phototherapy, *J. Colloid Interface Sci.*, **652**, 1108-1116, https://doi.org/10.1016/j.jcis.2023.08.126.
133. Melo, B. L., Lima-Sousa, R., Alves, C. G., Correia, I. J., and de Melo-Diogo, D. (2023) Sulfobetaine methacrylate-coated reduced graphene oxide-IR780 hybrid nanosystems for effective cancer photothermal-photodynamic therapy, *Int. J. Pharm.*, **647**, 123552, https://doi.org/10.1016/j.ijpharm.2023.123552.
134. Lima-Sousa, R., Melo, B. L., Mendonça, A. G., Correia, I. J., and de Melo-Diogo, D. (2024) Hyaluronic acid-functionalized graphene-based nanohybrids for targeted breast cancer chemo-photothermal therapy, *Int. J. Pharm.*, **651**, 123763, https://doi.org/10.1016/j.ijpharm.2023.123763.
135. Gao, J., Cao, C., Rui, Q., Sheng, Y., Cai, W., Li, J., and Kong, Y. (2023) A tri-responsive dual-drug delivery system based on mesoporous silica nanoparticles@polydopamine@graphene oxide nanosheets for chemo-photothermal therapy of osteosarcoma, *J. Saudi Chem. Soc.*, **27**, 101655, https://doi.org/10.1016/j.jscs.2023.101655.
136. Hosseinzadeh, R., Khorsandi, K., and Hosseinzadeh, G. (2018) Graphene oxide-methylene blue nanocomposite in photodynamic therapy of human breast cancer, *J. Biomol. Struct. Dyn.*, **36**, 2216-2223, https://doi.org/10.1080/07391102.2017.1345698.
137. Ma, M., Cheng, L., Zhao, A., Zhang, H., and Zhang, A. (2020) Pluronic-based graphene oxide-methylene blue nanocomposite for photodynamic/photothermal combined therapy of cancer cells, *Photodiagnosis. Photodyn. Ther.*, **29**, 101640, https://doi.org/10.1016/j.pdpdt.2019.101640.
138. Wei, Y., Zhou, F., Zhang, D., Chen, Q., and Xing, D. (2016) A graphene oxide based smart drug delivery system for tumor mitochondria-targeting photodynamic therapy, *Nanoscale*, **8**, 3530-3538, https://doi.org/10.1039/c5nr07785k.
139. Li, Y., Dong, H., Li, Y., and Shi, D. (2015) Graphene-based nanovehicles for photodynamic medical therapy, *Int. J. Nanomedicine*, **10**, 2451-2459, https://doi.org/10.2147/ijn.s68600.
140. Chen, Z., Li, Z., Wang, J., Ju, E., Zhou, L., Ren, J., and Qu, X. (2014) A multi-synergistic platform for sequential irradiation-activated high-performance apoptotic cancer therapy, *Adv. Funct. Mater.*, **24**, 522-529, https://doi.org/10.1002/adfm.201301951.
141. Chen, J., Wu, W., Zhang, F., Zhang, J., Liu, H., Zheng, J., Guo, S., and Zhang, J. (2020) Graphene quantum dots in photodynamic therapy, *Nanoscale Adv.*, **2**, 4961-4967, https://doi.org/10.1039/d0na00631a.
142. Ahirwar, S., Mallick, S., and Bahadur, D. (2020) Photodynamic therapy using graphene quantum dot derivatives, *J. Solid State Chem.*, **282**, 121107, https://doi.org/10.1016/j.jssc.2019.121107.
143. Ge, J., Lan, M., Zhou, B., Liu, W., Guo, L., Wang, H., Jia, Q., Niu, G., Huang, X., Zhou, H., Meng, X., Wang, P.,

Lee, C. S., Zhang, W., and Han, X. (2014) A graphene quantum dot photodynamic therapy agent with high singlet oxygen generation, *Nat. Commun.*, **5**, 4596, https://doi.org/10.1038/ncomms5596.

144. Tian, B., Wang, C., Zhang, S., Feng, L., and Liu, Z. (2011) Photothermally enhanced photodynamic therapy delivered by nano-graphene oxide, *ACS Nano*, **5**, 7000-7009, https://doi.org/10.1021/nn201560b.
145. Huang, P., Xu, C., Lin, J., Wang, C., Wang, X., Zhang, C., Zhou, X., Guo, S., and Cui, D. (2011) Folic acid-conjugated graphene oxide loaded with photosensitizers for targeting photodynamic therapy, *Theranostics*, **1**, 240-250, https://doi.org/10.7150/thno/v01p0240.
146. Zhou, L., Jiang, H., Wei, S., Ge, X., Zhou, J., and Shen, J. (2012) High-efficiency loading of hypocrellin B on graphene oxide for photodynamic therapy, *Carbon N Y*, **50**, 5594-5604, https://doi.org/10.1016/j.carbon.2012.08.013.
147. Wang, Y., Wang, H., Liu, D., Song, S., Wang, X., and Zhang, H. (2013) Graphene oxide covalently grafted upconversion nanoparticles for combined NIR mediated imaging and photothermal/photodynamic cancer therapy, *Biomaterials*, **34**, 7715-7724, https://doi.org/10.1016/j.biomaterials.2013.06.045.
148. Rong, P., Yang, K., Srivastan, A., Kiesewetter, D. O., Yue, X., Wang, F., Nie, L., Bhirde, A., Wang, Z., Liu, Z., Niu, G., Wang, W., and Chen, X. (2014) Photosensitizer loaded nano-graphene for multimodality imaging guided tumor photodynamic therapy, *Theranostics*, **4**, 229-239, https://doi.org/10.7150/thno.8070.
149. Cho, Y., Kim, H., and Choi, Y. (2013) A graphene oxide-photosensitizer complex as an enzyme-activatable theranostic agent, *Chem. Commun.*, **49**, 1202-1204, https://doi.org/10.1039/c2cc36297j.
150. Sahu, A., Choi, W. I., Lee, J. H., and Tae, G. (2013) Graphene oxide mediated delivery of methylene blue for combined photodynamic and photothermal therapy, *Biomaterials*, **34**, 6239-6248, https://doi.org/10.1016/j.biomaterials.2013.04.066.
151. Zhou, L., Zhou, L., Wei, S., Ge, X., Zhou, J., Jiang, H., Li, F., and Shen, J. (2014) Combination of chemotherapy and photodynamic therapy using graphene oxide as drug delivery system, *J. Photochem. Photobiol. B*, **135**, 7-16, https://doi.org/10.1016/j.jphotobiol.2014.04.010.
152. Gollavelli, G., and Ling, Y. C. (2014) Magnetic and fluorescent graphene for dual modal imaging and single light induced photothermal and photodynamic therapy of cancer cells, *Biomaterials*, **35**, 4499-4507, https://doi.org/10.1016/j.biomaterials.2014.02.011.
153. Yan, X., Hu, H., Lin, J., Jin, A. J., Niu, G., Zhang, S., Huang, P., Shen, B., and Chen, X. (2015) Optical and photoacoustic dual-modality imaging guided synergistic photodynamic/photothermal therapies, *Nanoscale*, **7**, 2520-2526, https://doi.org/10.1039/c4nr06868h.
154. Wu, C., Zhu, A., Li, D., Wang, L., Yang, H., Zeng, H., and Liu, Y. (2016) Photosensitizer-assembled PEGylated graphene-copper sulfide nanohybrids as a synergistic near-infrared phototherapeutic agent, *Expert Opin. Drug Deliv.*, **13**, 155-165, https://doi.org/10.1517/17425247.2016.1118049.
155. Yan, X., Niu, G., Lin, J., Jin, A. J., Hu, H., Tang, Y., Zhang, Y., Wu, A., Lu, J., Zhang, S., Huang, P., Shen, B., and Chen, X. (2015) Enhanced fluorescence imaging guided photodynamic therapy of sinoporphyrin sodium loaded graphene oxide, *Biomaterials*, **42**, 94-102, https://doi.org/10.1016/j.biomaterials.2014.11.040.
156. Kim, Y. K., Na, H. K., Kim, S., Jang, H., Chang, S. J., and Min, D. H. (2015) One-Pot synthesis of multifunctional Au@Graphene oxide nanocolloid Core@Shell nanoparticles for Raman bioimaging, photothermal, and photodynamic therapy, *Small*, **11**, 2527-2535, https://doi.org/10.1002/smll.201402269.
157. Luo, S., Yang, Z., Tan, X., Wang, Y., Zeng, Y., Wang, Y., Li, C., Li, R., and Shi, C. (2016) Multifunctional photosensitizer grafted on polyethylene glycol and polyethylenimine dual-functionalized nanographene oxide for cancer-targeted near-infrared imaging and synergistic phototherapy, *ACS Appl. Mater. Interfaces*, **8**, 17176-17186, https://doi.org/10.1021/acsami.6b05383.
158. Kalluru, P., Vankayala, R., Chiang, C. S., and Hwang, K. C. (2016) Nano-graphene oxide-mediated *in vivo* fluorescence imaging and bimodal photodynamic and photothermal destruction of tumors, *Biomaterials*, **95**, 1-10, https://doi.org/10.1016/j.biomaterials.2016.04.006.
159. Wo, F., Xu, R., Shao, Y., Zhang, Z., Chu, M., Shi, D., and Liu, S. (2016) A multimodal system with synergistic effects of magneto-mechanical, photothermal, photodynamic and chemo therapies of cancer in graphene-quantum dot-coated hollow magnetic nanospheres, *Theranostics*, **6**, 485-500, https://doi.org/10.7150/thno.13411.
160. Wu, C., Li, D., Wang, L., Guan, X., Tian, Y., Yang, H., Li, S., and Liu, Y. (2017) Single wavelength light-mediated, synergistic bimodal cancer photoablation and amplified photothermal performance by graphene/gold nanostar/photosensitizer theranostics, *Acta Biomater.*, **53**, 631-642, https://doi.org/10.1016/j.actbio.2017.01.078.
161. Gulzar, A., Xu, J., Yang, D., Xu, L., He, F., Gai, S., and Yang, P. (2018) Nano-graphene oxide-UCNP-Ce6 covalently constructed nanocomposites for NIR-mediated bioimaging and PTT/PDT combinatorial therapy, *Dalton Transactions*, **47**, 3931-3939, https://doi.org/10.1039/c7dt04141a.
162. Hatamie, S., Ahadian, M. M., Ghiass, M. A., Iraji zad, A., Saber, R., Parseh, B., Oghabian, M. A., and Shanehsazzadeh Zadeh, S. (2016) Graphene/cobalt nanocarrier for hyperthermia therapy and MRI diagnosis, *Colloids Surf. B Biointerfaces*, **146**, 271-279, https://doi.org/10.1016/j.colsurfb.2016.06.018.
163. Su, Y., Wang, N., Liu, B., Du, Y., Li, R., Meng, Y., Feng, Y., Shan, Z., and Meng, S. (2020) A phototheranostic nanoparticle for cancer therapy fabricated by BODIPY

and graphene to realize photo-chemo synergistic therapy and fluorescence/photothermal imaging, *Dyes Pigments*, **177**, 108262, https://doi.org/10.1016/j.dyepig.2020.108262.

164. Taratula, O., Patel, M., Schumann, C., Naleway, M. A., Pang, A. J., He, H., and Taratula, O. (2015) Phthalocyanine-loaded graphene nanoplatform for imaging-guided combinatorial phototherapy, *Int. J. Nanomedicine*, **10**, 2347, https://doi.org/10.2147/ijn.s81097.
165. Lamb, J., Fischer, E., Rosillo-Lopez, M., Salzmann, C. G., and Holland, J. P. (2019) Multi-functionalised graphene nanoflakes as tumour-targeting theranostic drug-delivery vehicles, *Chem. Sci.*, **10**, 8880-8888, https://doi.org/10.1039/c9sc03736e.
166. Tomasella, P., Sanfilippo, V., Bonaccorso, C., Cucci, L. M., Consiglio, G., Nicosia, A., Mineo, P. G., Forte, G., and Satriano, C. (2020) Theranostic nanoplatforms of thiolated reduced graphene oxide nanosheets and gold nanoparticles, *Appl. Sci.*, **10**, 5529, https://doi.org/10.3390/app10165529.
167. Usman, M. S., Hussein, M. Z., Fakurazi, S., Masarudin, M. J., and Saad, F. F. A. (2018) A bimodal theranostic nanodelivery system based on [graphene oxide-chlorogenic acid-gadolinium/gold] nanoparticles, *PLoS One*, **13**, e0200760, https://doi.org/10.1371/journal.pone.0200760.
168. Chawda, N., Basu, M., Majumdar, D., Poddar, R., Mahapatra, S. K., and Banerjee, I. (2019) Engineering of gadolinium-decorated graphene oxide nanosheets for multimodal bioimaging and drug delivery, *ACS Omega*, **4**, 12470-12479, https://doi.org/10.1021/acsomega.9b00883.
169. Samadian, H., Mohammad-Rezaei, R., Jahanban-Esfahlan, R., Massoumi, B., Abbasian, M., Jafarizad, A., and Jaymand, M. (2020) A de novo theranostic nanomedicine composed of PEGylated graphene oxide and gold nanoparticles for cancer therapy, *J. Mater. Res.*, **35**, 430-441, https://doi.org/10.1557/jmr.2020.3.
170. Yang, Y., Wang, S., Wang, C., Tian, C., Shen, Y., and Zhu, M. (2019) Engineered targeted hyaluronic acid-glutathione-stabilized gold nanoclusters/graphene oxide-5-fluorouracil as a smart theranostic platform for stimulus-controlled fluorescence imaging-assisted synergetic chemo/phototherapy, *Chem. As. J.*, **14**, 1418-1423, https://doi.org/10.1002/asia.201900153.
171. Guo, S., Song, Z., Ji, D.-K., Reina, G., Fauny, J.-D., Nishina, Y., Ménard-Moyon, C., and Bianco, A. (2022) Combined photothermal and photodynamic therapy for cancer treatment using a multifunctional graphene oxide, *Pharmaceutics*, **14**, 1365, https://doi.org/10.3390/pharmaceutics14071365.
172. Baktash, M. S., Zarrabi, A., Avazverdi, E., and Reis, N. M. (2021) Development and optimization of a new hybrid chitosan-grafted graphene oxide/magnetic nanoparticle system for theranostic applications, *J. Mol. Liq.*, **322**, 114515, https://doi.org/10.1016/j.molliq.2020.114515.
173. Pan, J., Yang, Y., Fang, W., Liu, W., Le, K., Xu, D., and Li, X. (2018) Fluorescent phthalocyanine-graphene conjugate with enhanced nir absorbance for imaging and multi-modality therapy, *ACS Appl. Nano Mater.*, **1**, 2785-2795, https://doi.org/10.1021/acsanm.8b00449.
174. Chen, M. L., Gao, Z. W., Chen, X. M., Pang, S. C., and Zhang, Y. (2018) Laser-assisted *in situ* synthesis of graphene-based magnetic-responsive hybrids for multimodal imaging-guided chemo/photothermal synergistic therapy, *Talanta*, **182**, 433-442, https://doi.org/10.1016/j.talanta.2018.02.030.
175. Chang, X., Zhang, Y., Xu, P., Zhang, M., Wu, H., and Yang, S. (2018) Graphene oxide/MnWO4 nanocomposite for magnetic resonance/photoacoustic dual-model imaging and tumor photothermo-chemotherapy, *Carbon N Y*, **138**, 397-409, https://doi.org/10.1016/j.carbon.2018.07.058.
176. Prasad, R., Yadav, A. S., Gorain, M., Chauhan, D. S., Kundu, G. C., Srivastava, R., and Selvaraj, K. (2019) Graphene oxide supported liposomes as red emissive theranostics for phototriggered tissue visualization and tumor regression, *ACS Appl. Bio Mater.*, **2**, 3312-3320, https://doi.org/10.1021/acsabm.9b00335.
177. Samiei Foroushani, M., Karimi Shervedani, R., Kefayat, A., Torabi, M., Ghahremani, F., and Yaghoobi, F. (2009) Folate-graphene chelate manganese nanoparticles as a theranostic system for colon cancer MR imaging and drug delivery: *in vivo* examinations, *J. Drug Deliv. Sci. Technol.*, **54**, 101223, https://doi.org/10.1016/j.jddst.2019.101223.
178. Luo, Y., Tang, Y., Liu, T., Chen, Q., Zhou, X., Wang, N., Ma, M., Cheng, Y., and Chen, H. (2019) Engineering graphene oxide with ultrasmall SPIONs and smart drug release for cancer theranostics, *Chem. Commun.*, **55**, 1963-1966, https://doi.org/10.1039/c8cc09185d.
179. Shi, S., Yang, K., Hong, H., Valdovinos, H. F., Nayak, T. R., Zhang, Y., Theuer, C. P., Barnhart, T. E., Liu, Z., and Cai, W. (2013) Tumor vasculature targeting and imaging in living mice with reduced graphene oxide, *Biomaterials*, **34**, 3002, https://doi.org/10.1016/j.biomaterials.2013.01.047.
180. Cheng, S. J., Chiu, H. Y., Kumar, P. V., Hsieh, K. Y., Yang, J. W., Lin, Y. R., Shen, Y. C., and Chen, G. Y. (2018) Simultaneous drug delivery and cellular imaging using graphene oxide, *Biomater Sci.*, **6**, 813-819, https://doi.org/10.1039/c7bm01192j.
181. Hu, D., Zhang, J., Gao, G., Sheng, Z., Cui, H., and Cai, L. (2016) Indocyanine green-loaded polydopamine-reduced graphene oxide nanocomposites with amplifying photoacoustic and photothermal effects for cancer theranostics, *Theranostics*, **6**, 1043-1052, https://doi.org/10.7150/thno.14566.
182. Turcheniuk, K., Dumych, T., Bilyy, R., Turcheniuk, V., Bouckaert, J., Vovk, V., Chopyak, V., Zaitsev, V.,

Mariot, P., Prevarskaya, N., Boukherroub, R., and Szunerits, S. (2015) Plasmonic photothermal cancer therapy with gold nanorods/reduced graphene oxide core/shell nanocomposites, *RSC Adv.*, **6**, 1600-1610, https://doi.org/10.1039/c5ra24662h.

183. Wang, L., Wang, M., Zhou, B., Zhou, F., Murray, C., Towner, R. A., Smith, N., Saunders, D., Xie, G., and Chen, W. R. (2019) PEGylated reduced-graphene oxide hybridized with Fe_3O_4 nanoparticles for cancer photothermal-immunotherapy, *J. Mater. Chem. B*, **7**, 7406-7414, https://doi.org/10.1039/c9tb00630c.
184. Bansal, S., Singh, J., Kumari, U., Kaur, I. P., Barnwal, R. P., Kumar, R., Singh, S., Singh, G., and Chatterjee, M. (2019) Development of biosurfactant-based graphene quantum dot conjugate as a novel and fluorescent theranostic tool for cancer, *Int. J. Nanomedicine*, **14**, 809-818, https://doi.org/10.2147/ijn.s188552.
185. Ko, N. R., Hong, S. H., Nafiujjaman, M., An, S. Y., Revuri, V., Lee, S. J., Kwon, I. K., Lee, Y. ky., and Oh, S. J. (2019) Glutathione-responsive PEGylated GQD-based nanomaterials for diagnosis and treatment of breast cancer, *J. Industr. Engin. Chem.*, **71**, 301-307, https://doi.org/10.1016/j.jiec.2018.11.039.
186. Li, S., Zhou, S., Li, Y., Li, X., Zhu, J., Fan, L., and Yang, S. (2017) Exceptionally high payload of the IR780 iodide on folic acid-functionalized graphene quantum dots for targeted photothermal therapy, *ACS Appl. Mater. Interfaces*, **9**, 22332-22341, https://doi.org/10.1021/acsami.7b07267.
187. Ding, H., Zhang, F., Zhao, C., Lv, Y., Ma, G., Wei, W., and Tian, Z. (2017) Beyond a carrier: graphene quantum dots as a probe for programmatically monitoring anti-cancer drug delivery, release, and response, *ACS Appl. Mater. Interfaces*, **9**, 27396-27401, https://doi.org/10.1021/acsami.7b08824.
188. Badrigilan, S., Shaabani, B., Gharehaghaji, N., and Mesbahi, A. (2019) Iron oxide/bismuth oxide nanocomposites coated by graphene quantum dots: "Three-in-one" theranostic agents for simultaneous CT/MR imaging-guided *in vitro* photothermal therapy, *Photodiagnosis Photodyn. Ther.*, **25**, 504-514, https://doi.org/10.1016/j.pdpdt.2018.10.021.
189. Badrigilan, S., Shaabani, B., Aghaji, N. G., and Mesbahi, A. (2020) Graphene quantum dots-coated bismuth nanoparticles for improved CT imaging and photothermal performance, *Int. J. Nanosci.*, **19**, 1850043, https://doi.org/10.1142/s0219581x18500436.
190. Lee, B., Stokes, G. A., Valimukhametova, A., Nguyen, S., Gonzalez-Rodriguez, R., Bhaloo, A., Coffer, J., and Naumov, A. V. (2023) Automated approach to *in vitro* image-guided photothermal therapy with top-down and bottom-up-synthesized graphene quantum dots, *Nanomaterials*, **13**, 805, https://doi.org/10.3390/nano13050805.
191. Sung, S. Y., Su, Y. L., Cheng, W., Hu, P. F., Chiang, C. S., Chen, W. T., and Hu, S. H. (2019) Graphene quantum dots-mediated theranostic penetrative delivery of drug and photolytics in deep tumors by targeted biomimetic nanosponges, *Nano Lett.*, **19**, 69-81, https://doi.org/10.1021/acs.nanolett.8b03249.
192. Xuan, Y., Zhang, R. Y., Zhao, D. H., Zhang, X. S., An, J., Cheng, K., Hou, X. L., Song, X. L., Zhao, Y. D., and Yang, X. Q. (2019) Ultrafast synthesis of gold nanosphere cluster coated by graphene quantum dot for active targeting PA/CT imaging and near-infrared laser/pH-triggered chemo-photothermal synergistic tumor therapy, *Chem. Engin. J.*, **369**, 87-99, https://doi.org/10.1016/j.cej.2019.03.035.
193. Wu, C., Guan, X., Xu, J., Zhang, Y., Liu, Q., Tian, Y., Li, S., Qin, X., Yang, H., and Liu, Y. (2019) Highly efficient cascading synergy of cancer photo-immunotherapy enabled by engineered graphene quantum dots/photosensitizer/CpG oligonucleotides hybrid nanotheranostics, *Biomaterials*, **205**, 106-119, https://doi.org/10.1016/j.biomaterials.2019.03.020.
194. Ruiyi, L., Zaijun, L., Xiulan, S., Jan, J., Lin, L., Zhiguo, G., and Guangli, W. (2020) Graphene quantum dot-rare earth upconversion nanocages with extremely high efficiency of upconversion luminescence, stability and drug loading towards controlled delivery and cancer theranostics, *Chem. Engin. J.*, **382**, 122992, https://doi.org/10.1016/j.cej.2019.122992.
195. Liu, H., Li, C., Qian, Y., Hu, L., Fang, J., Tong, W., Nie, R., Chen, Q., and Wang, H. (2020) Magnetic-induced graphene quantum dots for imaging-guided photothermal therapy in the second near-infrared window, *Biomaterials*, **232**, 119700, https://doi.org/10.1016/j.biomaterials.2019.119700.
196. Zhang, X., Ong'achwa Machuki, J., Pan, W., Cai, W., Xi, Z., Shen, F., Zhang, L., Yang, Y., Gao, F., and Guan, M. (2020) Carbon nitride hollow theranostic nanoregulators executing laser-activatable water splitting for enhanced ultrasound/fluorescence imaging and cooperative phototherapy, *ACS Nano*, **14**, 4045-4060, https://doi.org/10.1021/acsnano.9b08737.
197. Prasad, R., Jain, N. K., Yadav, A. S., Jadhav, M., Radharani, N. N. V., Gorain, M., Kundu, G. C., Conde, J., and Srivastava, R. (2021) Ultrahigh penetration and retention of graphene quantum dot mesoporous silica nanohybrids for image guided tumor regression, *ACS Appl. Bio Mater.*, **4**, 1693-1703, https://doi.org/10.1021/acsabm.0c01478.
198. Yang, Y., Wang, B., Zhang, X., Li, H., Yue, S., Zhang, Y., Yang, Y., Liu, M., Ye, C., Huang, P., and Zhou, X. (2023) Activatable graphene quantum-dot-based nanotransformers for long-period tumor imaging and repeated photodynamic therapy, *Adv. Mater.*, **35**, 2211337, https://doi.org/10.1002/adma.202211337.